Biomaterials 35 (2014) 4548–4556

Contents lists available at ScienceDirect

Biomaterials

journal homepage: www.elsevier.com/locate/biomaterials

siRNA delivery from triblock copolymer micelles with spatially-ordered compartments of PEG shell, siRNA-loaded intermediate layer, and hydrophobic core

Hyun Jin Kim [a], Kanjiro Miyata [b], Takahiro Nomoto [c], Meng Zheng [b], Ahram Kim [c], Xueying Liu [b], Horacio Cabral [c], R. James Christie [b], Nobuhiro Nishiyama [d], Kazunori Kataoka [a,b,c,e,*]

[a] Department of Materials Engineering, Graduate School of Engineering, The University of Tokyo, 7-3-1 Hongo, Bunkyo-ku, Tokyo 113-8656, Japan
[b] Center for Disease Biology and Integrative Medicine, Graduate School of Medicine, The University of Tokyo, 7-3-1 Hongo, Bunkyo-ku, Tokyo 113-0033, Japan
[c] Department of Bioengineering, Graduate School of Engineering, The University of Tokyo, 7-3-1 Hongo, Bunkyo-ku, Tokyo 113-8656, Japan
[d] Polymer Chemistry Division, Chemical Resources Laboratory, Tokyo Institute of Technology, R1-11, 4259 Nagatsuta, Midori-ku, Yokohama 226-8503, Japan
[e] Center for NanoBio Integration, The University of Tokyo, 7-3-1 Hongo, Bunkyo-ku, Tokyo 113-8656, Japan

ARTICLE INFO

Article history:
Received 11 December 2013
Accepted 9 February 2014
Available online 6 March 2014

Keywords:
siRNA delivery
Polyion complex micelle
Triblock copolymer
Hydrophobic interaction

ABSTRACT

Hydrophobized block copolymers have widely been developed for construction of polymeric micelles for stable delivery of nucleic acids as well as anticancer drugs. Herein, we elaborated an A-B-C type of triblock copolymer featuring shell-forming A-segment, nucleic acid-loading B-segment, and stable core-forming C-segment, directed toward construction of a three-layered polymeric micelle as a small interfering RNA (siRNA) vehicle. The triblock copolymer was prepared with nonionic and hydrophilic poly(ethylene glycol) (PEG), cationic poly(L-lysine) (PLys), and poly{*N*-[*N*-(2-aminoethyl)-2-aminoethyl] aspartamide} [PAsp(DET)] bearing a hydrophobic dimethoxy nitrobenzyl ester (DN) moiety in the side chain [PEG-PLys-PAsp(DET-DN)]. The resulting triblock copolymers spontaneously formed sub-100 nm-sized polymeric micelles with a hydrophobic PAsp(DET-DN) core as well as PEG shell in an aqueous solution. This micelle was able to incorporate siRNA into the intermediate PLys layer, associated with slightly reduced size and a narrow size distribution. The triblock copolymer micelles (TCMs) stably encapsulated siRNA in serum-containing medium, whereas randomly hydrophobized triblock copolymer [PEG-PLys(DN)-PAsp(DET-DN)] control micelles (RCMs) gradually released siRNA with time and non-PEGylated diblock copolymer [PLys-PAsp(DET-DN)] control micelles (DCMs) immediately formed large aggregates. The TCMs thus induced appreciably stronger sequence-specific gene silencing in cultured cancer cells, compared to those control micelles. The siRNA delivery with TCMs was further examined in terms of cellular uptake and intracellular trafficking. The flow cytometric analysis revealed that the cellular uptake of TCMs was more efficient than that of RCMs, but less efficient than that of DCMs. The intracellular trafficking study using confocal laser scanning microscopy combined with fluorescence resonance energy transfer (FRET) revealed that the TCMs could readily release the siRNA payload within cells, which was in contrast to the DCMs exhibiting much slower release profile. This result indicates that PEG shell contributed to the smooth release of siRNA from TCMs within the cells, presumably due to avoiding irreversible aggregate formation. The obtained results demonstrated that the design of separately functionalized polymer segments expanded the performance of polymeric micelles for successful siRNA delivery.

1. Introduction

Small interfering RNA (siRNA), a trigger of RNA interference (RNAi), offers a new therapeutic modality for various intractable diseases, including cancer. To fulfill successful RNAi therapy, siRNA

* Corresponding author. Department of Materials Engineering, Graduate School of Engineering, The University of Tokyo, 7-3-1 Hongo, Bunkyo-ku, Tokyo 113-8656, Japan.
E-mail address: kataoka@bmw.t.u-tokyo.ac.jp (K. Kataoka).

http://dx.doi.org/10.1016/j.biomaterials.2014.02.016
0142-9612/

has generated the need for development of delivery vehicles, due to its biologically unstable nature and inefficient cellular uptake [1–3]. In this regard, block copolymers of neutral and hydrophilic poly(ethylene glycol) (PEG) and polycation have been developed as a promising delivery platform. The block copolymers electrostatically bind to oppositely charged siRNA to form a polyion complex (PIC) micelle having a distinctive core–shell structure, *i.e.*, PIC core for protecting siRNA payloads from enzymatic degradations and PEG shell for providing enhanced colloidal stability and reducing unfavorable interactions with biomacromolecules [4–6]. In particular, a sub-100 nm size of PIC micelles is preferable to deliver siRNA into solid tumors through the tumoral leaky vasculature, namely enhanced permeability and retention (EPR) effect [4,7–9]. Meanwhile, the electrostatic associations between siRNA and polycationic segment in the PIC core are inevitably interfered under biological conditions containing abundant charged biomacromolecules as a counterpart. Thus, to compensate such compromised stability of PIC micelles, additional stabilization approaches are required for successful siRNA delivery under harsh *in vivo* conditions.

So far, several stabilization approaches of PIC micelles have been explored by integrating stabilizing moieties, such as disulfide crosslinking [10–12], cholesterol groups [13–16], and long alkyl chains (*e.g.* stearoyl group) [17–21], into the polycationic segment. In particular, hydrophobic moieties can assist the spontaneous assembly of PICs through hydrophobic interactions in aqueous solutions, rendering PIC micelles more resistant to dissociation. Indeed, hydrophobic moieties have been randomly installed into polycationic segment in block copolymers without any specific arrangement [17–21]. Those hydrophobized block copolymers stabilized siRNA-loaded PIC micelles, demonstrating significant therapeutic effects in animal disease models bearing subcutaneous cancer or ischemia-reperfusion injury [20,21]. However, this "random modification" strategy may not fully utilize hydrophobic interactions, because hydrophilic siRNA and cationic moieties coexisting in the core probably interfere with the segregation of hydrophobic components in the core, leading to the compromised minimization of interfacial energy between shell and core [22–24]. Thus, we assumed that exclusion of hydrophilic siRNA payloads as well as polycationic segment from hydrophobic core allowed for more stable micelle formation. In this regard, our previous study installed a hydrophobic cholesterol moiety into ω-end of block copolymers, and the cholesterol-installed PIC micelles were significantly stabilized against the rapid dissociation in serum-containing medium [16]. Nevertheless, their moderate gene silencing efficiency *in vivo* suggested the necessity of further optimization of hydrophobic structures for improving the micelle performance.

An A-B-C type of triblock copolymer is a promising candidate for construction of polymeric micelles equipped with optimized hydrophobic core, because the C-segment can be elaborated with a variety of hydrophobic units. Thus, we herein synthesized a well-defined A-B-C triblock copolymer having hydrophilic PEG (A-segment), siRNA-loading cationic poly(L-lysine) (PLys) (B-segment), and hydrophobic core-forming polyaspartamide derivative (C-segment) (Fig. 1A). PLys having a high pK_a of ~10.5 was chosen to stably incorporate a negatively charged siRNA [25], as its binding affinity to nucleic acids is known to be relatively strong under biological conditions [26–28]. Also, polyaspartamide derivatives were prepared to regulate the hydrophobicity for enhanced micelle stability as well as uniform micelle formation, utilizing the aminolysis reaction with low molecular weight amine compounds [29]. The obtained triblock copolymers were characterized on their self-assembling behavior with or without siRNA in terms of size and its distribution. The triblock copolymer micelles (TCMs) were then examined on their stability in comparison with "randomly" hydrophobized control micelles (RCMs) (Fig. 1B) and non-PEGylated diblock copolymer control micelles (DCMs) (Fig. 1C). Cellular delivery of siRNA by those micelles was further compared in terms of the efficiencies of gene silencing, cellular uptake, and intracellular payload release, demonstrating the crucial roles of separately functionalized segments in TCMs for successful siRNA delivery.

2. Materials and methods

2.1. Materials

β-Benzyl-L-aspartate *N*-carboxy-anhydride (BLA-NCA) and ε-trifluoroacetyl-L-lysine *N*-carboxy anhydride [Lys(TFA)-NCA] were purchased from Chuo Kaseihin Co., Inc. (Tokyo, Japan). α-Methoxy-ω-amino-PEG (PEG-NH_2, M_n = 12,000) was obtained from NOF Co., Ltd. (Tokyo, Japan). *N,N*-Dimethylformamide (DMF), dichloromethane, diethylenetriamine (DET), methanol (MeOH), dimethylsulfoxide (DMSO), thiourea, diethylether, and *N*-methyl-2-pyrrolidone (NMP) were purchased from Wako Pure Chemical Industries, Ltd. (Osaka, Japan). Dulbecco's modified Eagle's medium (DMEM), diisopropylethylamine (DIPEA), and 4,5-dimethoxy-2-nitrobenzylchloroformate were purchased from Sigma–Aldrich Co. (St. Louis, MO). HEPES (1 M, pH 7.3) was purchased from Amresco (Solon, OH). DMF, DMSO, NMP, DET, and DIPEA were distilled with the conventional methods before use. Fetal bovine serum (FBS) and Alexa488-, Alexa546-, or Alexa647-labeled firefly luciferase siRNA (siLuc) were purchased from Invitrogen (Carlsbad, CA). Non-labeled siLuc (sense: 5′-CUU ACG CUG AGU ACU UCG AdTdT-3′; antisense: 5′-UCG AAG UAC UCA GCG UAA GdTdT-3′) and control siRNA (siCon) (sense: 5′-UUC UCC GAA CGU GUC ACG UdTdT-3′; antisense: 5′-ACG UGA CAC GUU CGG AGA AdTdT-3′) were synthesized by Hokkaido System Science Co., Ltd. (Hokkaido, Japan).

2.2. Synthesis of PEG-PLys(TFA)-PBLA

PEG-NH_2 (306 mg, 25.5 μmol) dissolved in DMF containing 1 M thiourea (DMF/thiourea, 4.5 mL) was added to Lys(TFA)-NCA solution (479 mg, 1.78 mmol) dissolved in DMF/thiourea (7.5 mL) [30]. The polymerization proceeded at 35 °C for 48 h under argon atmosphere. The resulting diblock copolymer was precipitated in diethylether three times and dried under reduced pressure overnight. The degree of polymerization (DP) of the Lys(TFA) unit was calculated to be 57 from ^{1}H NMR spectrum (10 mg/mL, 80 °C) based on the peak intensity ratio of the β, γ, and δ-methylene protons of lysine (–$(CH_2)_3$–, δ = 1.4–1.8) to the oxyethylene protons of PEG (–(OCH_2CH_2)–, δ = 3.7). For triblock copolymer, PEG-PLys(TFA) (300 mg, 12.2 μmol) in DMSO containing 1 M thiourea (DMSO/thiourea, 4.5 mL) was added to BLA-NCA solution (54.2 mg, 219 μmol) dissolved in DMSO/thiourea (1 mL). The polymerization proceeded at 35 °C for 48 h under argon atmosphere. The resulting triblock copolymer was precipitated in diethylether and dried under reduced pressure overnight. The DP of the BLA unit was calculated to be 18 from ^{1}H NMR spectrum (10 mg/mL, 80 °C) based on the peak intensity ratio between phenyl protons ($C_6H_5CH_2$–, δ = 7.3) in PBLA and ethylene protons (–(OCH_2CH_2)–, δ = 3.7) in PEG. The triblock copolymer was further characterized by gel permeation chromatography (GPC) (HLC-8220, TOSOH Corporation, Tokyo, Japan) equipped with two TSK gel columns (TSK-gel Super AW4000 and Super AW3000) through DMF containing LiCl (10 mM) at 0.8 mL/min. Molecular weight distribution (M_w/M_n) of the triblock copolymer was determined to be 1.08.

2.3. Synthesis of PEG-PLys(TFA)-PAsp(DET)

PEG-PLys(TFA)-PAsp(DET) (2) was prepared by the aminolysis reaction of PBLA with DET (Scheme S1) [18]. Briefly, PEG-PLys(TFA)-PBLA (1) (173 mg) was dissolved in NMP containing 1 M thiourea (NMP/thiourea, 8 mL) at 35 °C and cooled to 4 °C. Next, DET (0.6 mL) was diluted with NMP/thiourea (1.2 mL) and PEG-PLys(TFA)-PBLA solution was added dropwise into the DET solution. The mixture was stirred for 1 h at 15 °C under argon atmosphere. Then, the reaction mixture was added dropwise into ice-cold 5 M HCl (5 mL) for neutralization. The polymer product was purified by dialysis against 0.01 M HCl overnight and then deionized water for 2 h at 4 °C. The dialyzed solution was lyophilized to obtain the final product.

2.4. DN Introduction into DET moiety in PEG-PLys(TFA)-PAsp(DET)

First, a solution of PEG-PLys(TFA)-PAsp(DET) (2) (80 mg, 2.71 μmol) and distilled DIPEA (41 μL, 244 μmol) was prepared in MeOH/dichlorometane (4 mL, 1:1 v/v). Next, a solution of 4,5-dimethoxy-2-nitrobenzylchloroformate (26.9 mg, 0.0975 mmol) in dichlorometane (2 mL) was added dropwise to the PEG-PLys(TFA)-PAsp(DET) solution and the mixture was stirred for 24 h at 4 °C in the dark. The reaction was stopped by precipitation in diethylether (120 mL) and crude product was isolated by filtration. The filtered product was dissolved in MeOH/water (1:1 v/v) and dialyzed at 4 °C against 0.01 M HCl overnight and deionized water for 2 h in the dark. The final product was obtained by lyophilization.

2.5. Deprotection of TFA moiety in PEG-PLys(TFA)-PAsp(DET-DN)

PEG-PLys(TFA)-PAsp(DET-DN) (3) (60 mg) was dissolved in a mixed solvent of methanol (9 mL) and 1 N NaOH solution (1 mL) for 8 h at 35 °C. The mixture was

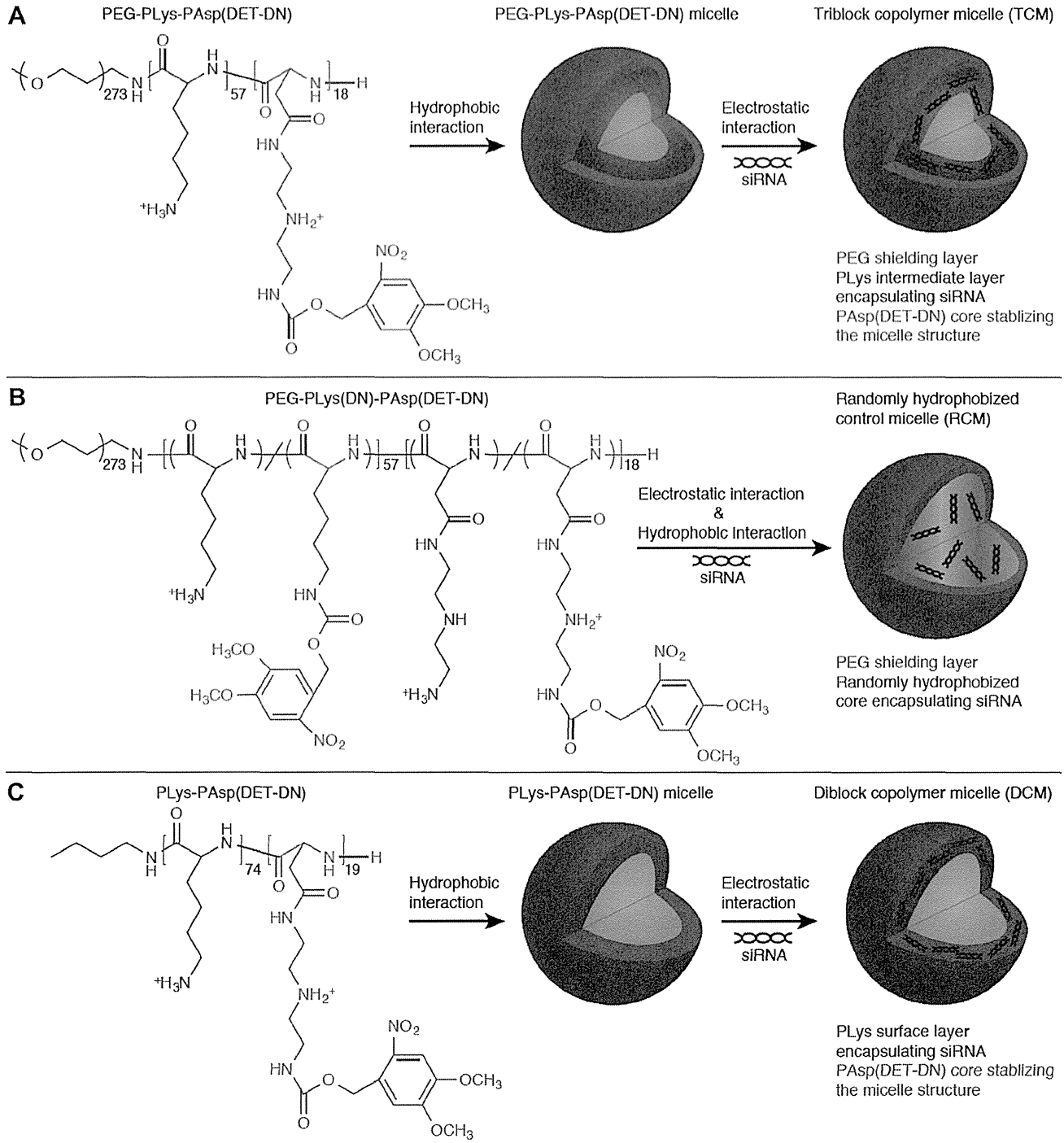

Fig. 1. Chemical structures of block copolymers developed in this study and schematic illustrations of hydrophobic triblock copolymer micelle (TCM; A), randomly hydrophobized control micelle (RCM; B), and diblock copolymer micelle without PEG shell (DCM; C).

dialyzed against 0.01 N HCl and then against deionized water. The final solution was lyophilized to obtain PEG-PLys-PAsp(DET-DN) (4) in the chloride salt form. The deprotection of the TFA groups was confirmed by ^{1}H NMR from the peak ratio of the methylene protons adjacent to the ε-amino group.

^{1}H NMR (D_2O/CD_3COOD): δ1.4–δ1.8 (342.9H, $COCH(CH_2)_3CH_2NH_3Cl$), δ2.7 (23.2H, $CHCH_2CONH$), δ3.0 (111.9H, $(CH_2)_3CH_2NH_3Cl$), δ3.3–δ3.4 (101.1H, $NH(CH_2)_2NH(CH_2)_2NH$), δ3.6 (1090H, OCH_2CH_2), δ3.8 (55.8H, $COCH_3COCH_3$), δ4.4 (56.5H, COCHNH), δ4.7 (14.0H, COCHNH), δ6.8 (26.0H, $CHCOCH_3COCH_3$), δ7.4 (24.1H, $COCH_3CHCNO_2$).

2.6. Micelle formation and siRNA loading

Polymeric micelles were prepared with PEG-PLys-PAsp(DET-DN) [or PLys-PAsp(DET-DN) as a non-PEGylated control] in an aqueous solution. The polymer (1 mg) was dissolved in 10 mM HEPES buffer (pH 7.3, 1 mg/mL) and incubated for 1 h in room temperature. Loading of siRNA in the polymeric micelles was performed by incubation of siRNA (20 μM in 10 mM HEPES buffer, pH 7.3) with the preformed polymeric micelles at the designated Amine/Phosphate ratios for 1–2 h in room temperature. The Amine/Phosphate ratio was defined as a residual molar ratio of

[primary amines in PEG-PLys-PAsp(DET-DN)]/[phosphates in siRNA]. Micelle size was determined at 25 °C using a Zetasizer (Malvern Instruments, Worcestershire, UK) equipped with a He–Ne Laser ($\lambda = 633$ nm) for the incident beam at a detection angle of 173°. Sample solutions were loaded into a low-volume quartz cuvette (ZEN2112, Malvern Instruments). The obtained data were analyzed by the cumulant method and the hydrodynamic (or cumulant) diameter of the micelles was then calculated by the Stokes–Einstein equation.

2.7. Transmission electron microscopy (TEM)

The shapes of micelles with or without siRNA were observed by a transmission electron microscope (JEM-1400, JEOL, Japan) operated with 100 kV acceleration voltages associated with 40 μA beam current. Micelle samples were placed on 400-mesh copper grids and stained using uranyl acetate solution (2% w/v).

2.8. Gel retardation assay

Gel electrophoresis was performed using 20% Novex polyacrylamide TBE gel (Invitrogen) under 100 V constant voltages for 60 min and then the gel was stained with SYBR Green II RNA Gel Stain (Invitrogen). Gels were imaged using Molecular Imager FX (Bio-Rad, Hercules, CA).

2.9. Fluorescence correlation spectroscopy (FCS)

FCS analyses were performed using a confocal laser scanning microscope, LSM510 (Carl Zeiss, Jena, Germany) equipped with a Confocor3 module and a Zeiss C-Apochromat 40 × water objective. A He–Ne laser (633 nm) was used for excitation of Alexa647-labeled siRNA and the emission was detected through above 650 nm. Samples were placed into an 8-well Lab-Tek chambered borosilicate cover-glass (Nalge Nunc International, Rochester, NY) and measured at room temperature. Stability of micelles containing Alexa647-labeled siRNA was evaluated in PBS containing 10% FBS (PBS/FBS). siRNA-loaded micelle solution (5 μM siRNA, Amine/Phosphate = 3) was diluted up to 100 nM siRNA with PBS/FBS, and then incubated at 37 °C for the designed period before measurements. Rhodamine 6G was used as a reference in 10 mM HEPES buffer (pH 7.3) to obtain a structural parameter in FCS analyses. Autocorrelation curves obtained from 10 measurements at a sampling time of 10 s were fitted with the Zeiss Confocor3 software package to calculate a diffusion coefficient of Alexa647-labeled siRNA.

2.10. In vitro luciferase gene silencing in cultured HeLa cells

Human cervical cancer cells stably expressing luciferase (HeLa-Luc) were seeded in 35 mm petri dishes (25,000 cells/dish) in DMEM containing 10% FBS (DMEM/FBS) and allowed to attach overnight. Then, the medium was removed and replaced with a fresh medium (2 mL) containing 100 μM luciferin and micelles (200 nM siRNA, Amine/Phosphate = 3). For each analysis, control samples were prepared by addition of medium diluted with 10 mM HEPES buffer (pH 7.3) instead of micelle solution. The added luciferin and micelle solution was 80 μL per 2 mL of medium. Samples were placed into a real-time photon-countable incubator (AB-2550 Kronos Dio, ATTO Corporation, Tokyo, Japan) and the luminescence intensity was measured periodically over 50 h at a temperature and CO_2 maintained at 37 °C and 5%, respectively. Relative luminescence intensity was determined by dividing the average luminescence intensity of treated samples by that of control samples ($n = 3$).

2.11. Cell viability assay

Cell viability was evaluated using a Cell Counting Kit-8 (Dojindo, Kumamoto, Japan). HeLa-Luc cells were seeded in a 96-well plate (5000 cells/well) in DMEM/FBS. After overnight incubation, siRNA-loaded micelles (Amine/Phosphate = 3) were added to the cells, and the cells were then incubated for 48 h. The micelle-containing medium was exchanged with a fresh medium (100 μL) containing the kit solution (10 μL), and the cells were further incubated for 1.5 h. The absorbance of the medium was measured at 450 nm using a microplate reader (Bio-Rad, Hercules, CA).

2.12. Flow cytometer measurement

HeLa-Luc cells were seeded in a 6-well plate (100,000 cells/well) in DMEM/FBS. Alexa647-labeled siRNA-loaded micelles were prepared with each polymer and added at 200 nM siRNA. After 4 h and 24 h incubation, the cells were washed twice with 0.5 mL of PBS, treated with a trypsin-EDTA solution, and suspended in PBS. The cellular uptake of siRNA-loaded micelles was measured using a flow cytometer (BD™ LSR II, BD Biosciences, San Jose, CA).

2.13. CLSM observation using FRET

HeLa-Luc cells (50,000 cells) were seeded in a 35-mm glass-based dish (Iwaki, Tokyo, Japan) and incubated overnight in DMEM/FBS. The micelles prepared with Alexa488-labeled siRNA and Alexa546-labeled siRNA (1:1 in molar ratio) at Amine/Phosphate = 3 were applied to the cells at 200 nM siRNA in fresh DMEM/FBS. Spectral images of the cells were obtained by LSM780 (Carl Zeiss, Oberkochen, Germany) equipped with a Plan-Apochromat 63 × objective (numerical aperture: 1.4) and the cells were incubated during CLSM observation in the incubator (Tokai Hit Co., Ltd., Shizuoka, Japan) at a temperature of 37 °C and a CO_2 concentration of 5%. The excitation wavelength was 488 nm (Ar laser) and the emission wavelength was 489–657 nm with the wavelength resolution of 8.8 nm. The spectral images were linearly unmixed into Alexa488 signal and Alexa546 signal, and FRET ratios in each pixel (Alexa546 signal/Alexa488 signal × 500) were calculated and expressed in a rainbow scale. All the image analyses were performed using ZEN software (Carl Zeiss).

Table 1
Hydrodynamic size, PDI, and ζ-potential of polymeric micelles without or with siRNA (Amine/Phosphate = 3).

Micelle	Polymer	Size (nm)/PDI/ζ-potential (mV) Without siRNA	Size (nm)/PDI/ζ-potential (mV) With siRNA
DCM	PLys-PAsp (DET-DN)	55/0.07/18.6	43/0.06/0.11
TCM	PEG-PLys-PAsp (DET-DN)	68/0.08/5.86	57/0.04/0.05
RCM	PEG-PLys(DN)-PAsp(DET-DN)	N.D.[a]	45/0.09/0.04

[a] The values were not determined due to substantially low scattered light intensity.

3. Results and discussion

3.1. Synthesis of block copolymers and their micelle characterizations

For construction of TCMs composed of hydrophilic shell, siRNA-loaded intermediate layer, and hydrophobic core, an A-B-C type of triblock copolymer was synthesized to have nonionic and hydrophilic PEG, cationic PLys, and hydrophobic polyaspartamide derivative (Fig. 1A). As a precursor, PEG-PLys(TFA)-PBLA was firstly synthesized by the sequential ring-opening polymerization of Lys(TFA)-NCA and then BLA-NCA, initiated by PEG-NH_2 as a macroinitiator (Scheme S1). The DP of PLys(TFA) and PBLA in the obtained triblock copolymer was determined to be 57 and 18, respectively, from ^{1}H NMR spectrum (Fig. S1). The DP of PLys(TFA) was designed to completely neutralize the negative charges of single siRNA (40 in 21mer/21mer) with single PLys chain. On the other hand, the DP of PBLA was targeted to be approximately 20, because our previous study revealed that the cationic polyaspartamide derivative modified with approximately 20 hydrophobic units significantly stabilized siRNA-loaded PICs in cell culture media [18]. The PBLA segment in PEG-PLys(TFA)-PBLA was aminolysed with DET, and then, the obtained PAsp(DET) segment was further modified with hydrophobic 4,5-dimethoxy-2-nitrobenzylchloroformate (DN) (Fig. 1A). The Asp(DET-DN) was developed here as a hydrophobic unit, because it enabled the micelle formation with a sub-100 nm size and a narrow size distribution, as demonstrated below. It should be noted that the utilization of ethylenediamine (–$NHCH_2CH_2NH$–) and triethylenetetramine [–$NH(CH_2CH_2NH)_3$–] linkers instead of DET [–$NH(CH_2CH_2NH)_2$–] resulted in larger micelle formation (>200 nm in diameter) associated with a larger size distribution [polydispersity index (PDI) in dynamic light scattering (DLS) > 0.1] (data not shown). These results suggest that fine-tuning of hydrophobic structures is crucial for the well-defined micelle formation. It should be further noted that the DN moiety is known to permit the carbamate cleavage via UV-irradiation, thus having the potential for external stimuli-responsive delivery [31,32]. Meanwhile, in order to verify the efficacy of hydrophobic C-segment on micelle stability, a control triblock copolymer, PEG-PLys(DN)-PAsp(DET-DN), was also synthesized by randomly introducing total 20 units of DN moieties into both PLys and PAsp(DET) segments (Fig. 1B). In addition, another control diblock copolymer, PLys-PAsp(DET-DN),

was synthesized from PLys(TFA)-PBLA for evaluating the effect of PEG on micelle properties (Fig. 1C).

Polymeric micelle formation with the obtained block copolymers was firstly evaluated in the absence of siRNA by DLS and ζ-potential measurements (Table 1) and TEM imaging (Fig. 2A). PEG-PLys-PAsp(DET-DN) successfully formed polymeric micelles having a cumulant diameter of 68 nm, a narrow size distribution (PDI = 0.08), and a moderately positive ζ-potential (~6 mV) in 10 mM HEPES buffer (pH 7.3). The narrow size distribution was also confirmed from the TEM image, which displays uniform and spherical structures having a number-averaged size of 20 ± 3 nm (n = 50). Considering that condensed nanostructures as well as phenyl derivatives can be effectively stained by uranyl acetate [33], these observed nanostructures are reasonably considered as a hydrophobic core composed of PAsp(DET-DN) segments. In a similar manner, PLys-PAsp(DET-DN) formed non-PEGylated diblock copolymer micelles that had a cumulant diameter of 55 nm, a PDI of 0.06, and a considerably positive ζ-potential (~19 mV) (Table 1). These results demonstrate that PAsp(DET-DN) segment with the DP of approximately 20 provided sufficient hydrophobicity to the block copolymers for micelle formation in aqueous solutions. It should be noted that the size and ζ-potential of PEG-PLys-PAsp(DET-DN) micelles were larger and lower, respectively, than those of PLys-PAsp(DET-DN) micelles, consistent with the presence of nonionic PEG shell in PEG-PLys-PAsp(DET-DN) micelles. On the other hand, the randomly hydrophobized triblock copolymer, PEG-PLys(DN)-PAsp(DET-DN), did not form such self-assemblies, as evidenced by a substantially lower scattered light intensity compared to PEG-PLys-PAsp(DET-DN) and PLys-PAsp(DET-DN) (Table S1). Taken together, it is indicated that a certain amount of sequential hydrophobic moieties in C-segment may be crucial for stable micelle formation with a hydrophobic core.

Next, siRNA was loaded into polymeric micelles by mixing siRNA solution with each micelle solution [or polymer solution for PEG-PLys(DN)-PAsp(DET-DN)]. The siRNA loading was confirmed by gel electrophoresis at various molar ratios of [primary amines in block copolymer]/[phosphates in siRNA] (Amine/Phosphate) ratios. Free siRNA band was not observed at Amine/Phosphate > 2 in TCMs and DCMs (Fig. S2), indicating complete encapsulation of siRNA within polymeric micelles. The cumulant size and ζ-potential of TCMs were decreased to 57 nm and 0.05 mV, respectively, and the narrow size distribution (PDI = 0.04) was maintained after polyionic complexation with siRNA at Amine/Phosphate = 3 (Table 1).

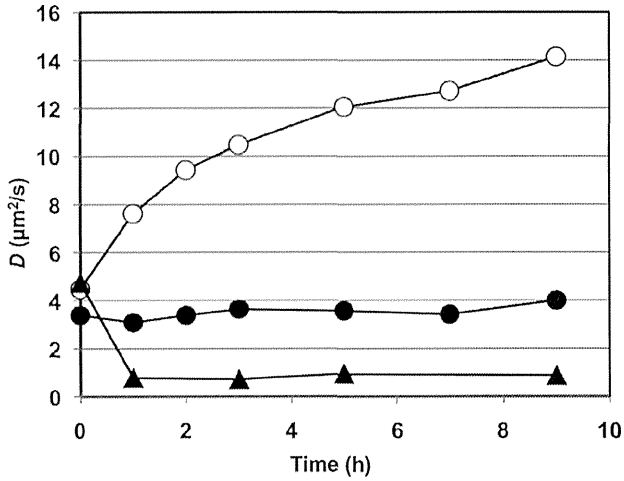

Fig. 3. Time-dependent changes in diffusion coefficient (D) of Alexa647-labeled siRNA loaded by DCMs (closed triangles), TCMs (closed circles), and RCMs (open circles) in PBS containing 10% FBS, measured by FCS.

Note that the similar cumulant size and size distribution were observed for the TCMs prepared at Amine/Phosphate ratios of 4 and 5 (Table S2), indicating that the well-defined micelle formation was not limited at a specific mixing ratio. The TEM image of siRNA-loaded TCMs depicts the formation of uniform and spherical nanostructures having a number-averaged size of 19 ± 2 nm (n = 50) (Fig. 2B). The similar complexation behavior was observed for the DCMs, which had the decreased cumulant size (43 nm) and ζ-potential (0.11 mV), associated with the low PDI of 0.06 (Table 1). These results indicate that negatively charged siRNAs were successfully bound to oppositely charged PLys segment within the preformed polymeric micelles without inducing secondary associations among the micelles. The almost similar sizes observed in the TEM images of TCMs with or without siRNA suggest that the hydrophobic PAsp(DET-DN) core should remain the same after the polyionic complexation. In contrast, the reduced cumulant sizes in the DLS analyses can be explained by shrinkage of the intermediate PLys layer in TCMs (or the outer layer in DCMs) through the polyionic complexation, presumably due to compromised electrostatic repulsion [34]. Altogether, the obtained results are consistent with our assumption that the TCMs should have the three-layered

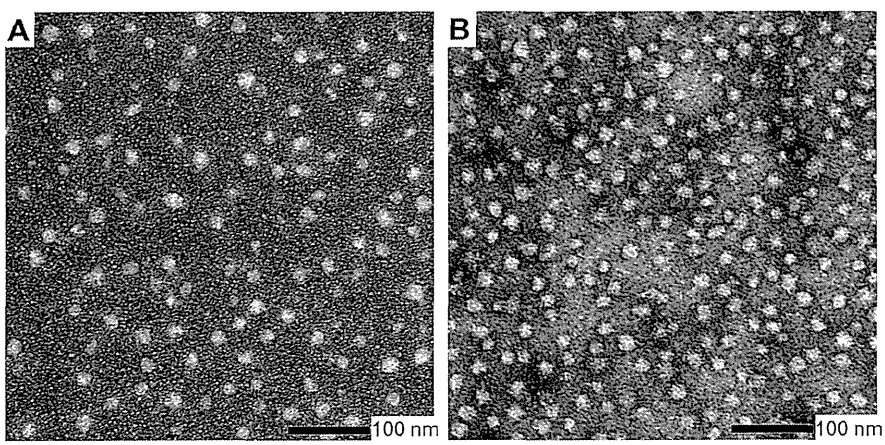

Fig. 2. TEM images of PEG-PLys-PAsp(DET-DN) micelles in the absence of siRNA (A) and in the presence of siRNA at Amine/Phosphate = 3 (B). Histograms of number-averaged size distribution of these TEM images were shown in Fig. S3. Scale bar represents 100 nm.

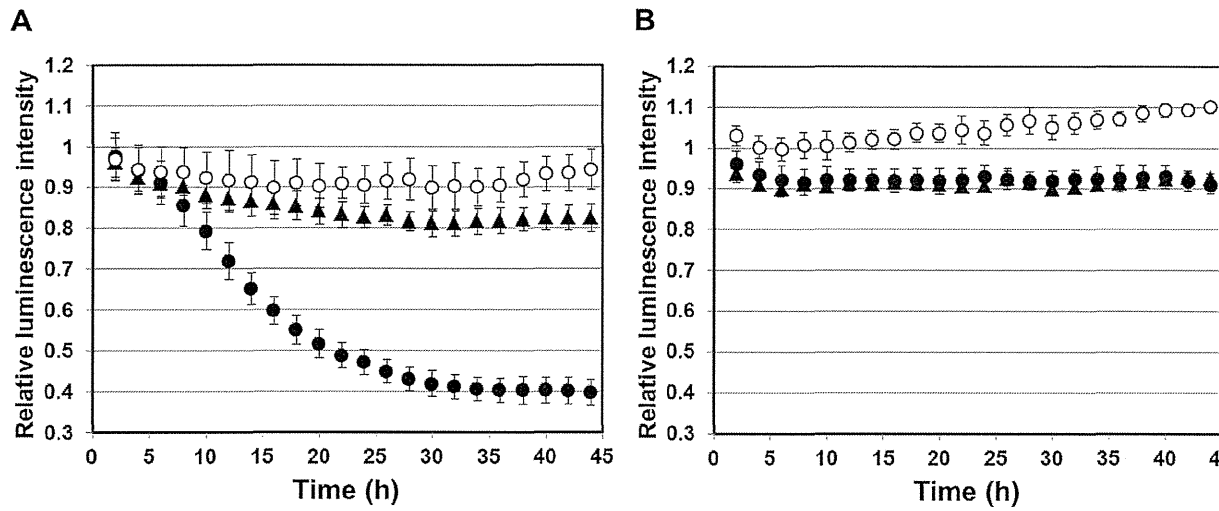

Fig. 4. Time dependent luciferase gene silencing of siRNA-loaded micelles, DCMs (closed triangles), TCMs (closed circles), and RCMs (open circles), in HeLa-Luc cells at 200 nM siRNA. A) siLuc and B) siCon. Results are expressed as the mean ± S.D. ($n = 3$).

structure featuring a hydrophobic core with the size of ~20 nm, siRNA/PLys PIC-based intermediate layer, and nonionic/hydrophilic PEG shell, as described in previous studies utilizing triblock copolymers composed of three different segments with varied electrostatic nature [35–38]. Meanwhile, PEG-PLys(DN)-PAsp(DET-DN) successfully formed PIC micelles (RCMs) with siRNA at Amine/Phosphate = 3 (Fig. S2), where their cumulant size, PDI, and ζ-potential were 45 nm, 0.09, and 0.04 mV, respectively (Table 1), through the charge-neutralization between the block copolymers and siRNAs. Based on the complete complexation of siRNA with a smaller amount of excess block copolymers, the micelle samples prepared at Amine/Phosphate = 3 were used in the following characterizations.

It was assumed that the micelle formation associated with the hydrophobic core should lead to higher stability in biological media containing charged biomacromolecules. Thus, the micelle stability in PBS/FBS was evaluated in terms of the change in diffusion coefficient (D), which was determined by FCS using fluorescently labeled siRNAs [16,18,19,28]. The micelle samples prepared with Alexa647-labeled siRNA at Amine/Phosphate = 3 were diluted with PBS/FBS, followed by the FCS measurement at different time points (Fig. 3). The initial D values of micelle samples (i.e. RCM, TCM, and DCM) were obviously lower than that of naked siRNA (56 ± 1 $\mu m^2/s$), consistent with the micelle formation between siRNAs and block copolymers. The D of RCMs gradually increased with time over 9 h, indicating micelle dissociation or siRNA release from the micelles. In contrast, the TCMs maintained their initial D over the incubation time, demonstrating the enhanced micelle stability in the culture medium due to the tightly packed hydrophobic core. The D of DCMs without PEG decreased immediately after dilution with PBS/FBS, indicating larger aggregate formation through adsorption of charged proteins onto the DCM surface. Altogether, it is concluded that both hydrophobic core and PEG shell should be essential for maintaining the siRNA-loaded micelle structure in the biological medium. The comparison of TCMs with previously reported, cholesterol-installed block copolymer micelles revealed the higher stability of TCMs, as indicated by the result that the D of the cholesterol-installed micelles reached that of naked siRNA after 1.5 h incubation in PBS/FBS [16]. The PAsp(DET) segment modified with sequentially-arranged 20 units of hydrophobic DN moieties would generate greater hydrophobicity compared to the single cholesterol moiety.

3.2. Cellular delivery of siRNA-loaded polymeric micelles

The gene silencing activity of siRNA-loaded micelles (Amine/Phosphate = 3) was investigated in cultured human cervical cancer cells stably expressing luciferase (HeLa-Luc). The luciferase-based luminescence intensity from the cells treated with each micelle was measured as an indicator of gene silencing by a photon-counting incubator (Fig. 4). Obviously, the TCMs showed the highest sequence-specific gene silencing efficiency among the tested micelles. In the cells treated with TCMs loading siLuc, the relative luminescence intensity progressively decreased with time and reached a plateau in approximately 30 h incubation. On the contrary, the TCMs loading siCon induced almost no decrease in relative luminescence intensity. Also, no significant cytotoxicity was observed in the cells treated with TCMs even at a high concentration of siRNA (2 μM) (Fig. S4), excluding the possibility of toxic effects on the decrease in luminescence intensity by TCMs with siLuc. On the other hand, DCMs and RCMs showed fairly weak gene silencing efficiency, compared to the TCMs (Fig. 4).

In order to elucidate the reason for the different gene silencing profiles among the tested micelles, a cellular uptake study was performed by a flow cytometer. Each micelle prepared with Alexa647-labeled siRNA (Amine/Phosphate = 3) was incubated with HeLa-Luc cells for 4 h and 24 h, and then the fluorescence intensity from the cells was measured (Fig. 5). All the micelle samples were more efficiently uptaken by the cells, compared to naked siRNA, presumably because of the adsorption and/or the partial exposure of polycationic segment contained in the micelles onto the oppositely charged cellular surface. In detail, RCMs and DCMs showed lower and higher cellular uptake efficiency, respectively, compared to TCMs at both time points. The lower cellular uptake of RCMs is probably due to their lower micelle stability in the serum-containing medium, as indicated in Fig. 3. The RCMs might gradually dissociate or release siRNA in the transfection medium, resulting in the compromised cellular entry of siRNA. This result is consistent with the appreciably lower gene silencing efficiency of RCMs, compared to TCMs. Meanwhile, the higher cellular uptake of DCMs might be explained by their non-PEGylated surface, which more likely facilitates the micelle adsorption onto the negatively charged cellular surface [39]. However, the efficient cellular uptake of DCMs is apparently inconsistent with their weak gene silencing efficiency in Fig. 4A. Thus, further studies are

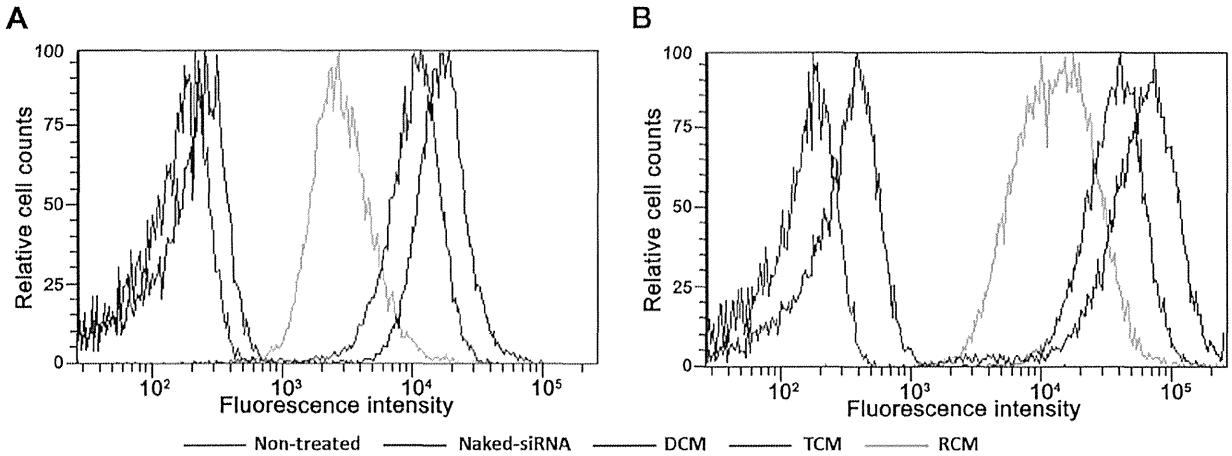

Fig. 5. Cellular uptake of Alexa647-labeled siRNA-loaded micelles (200 nM siRNA concentration, Amine/Phosphate = 3) in HeLa-Luc cells in 4 h (A) and 24 h (B) incubation.

required to explain about the different gene silencing efficiencies between TCMs and DCMs.

It is known that the transfer of siRNA from the endosome/lysosome to the cytoplasm is one of the critical steps for efficient gene silencing. Hence, the intracellular trafficking of fluorescently labeled siRNA-loaded micelles was examined by CLSM. Firstly, the colocalization of Alexa647-labeled siRNA with LysoTracker (Molecular Probes, Eugene, OR) that stains acidic cellular compartments (*i.e.* late endosome and lysosome) was observed after 24 h incubation as an indicator of endosomal escape efficiency (Fig. S5). Interestingly, there was no significant difference in the colocalization ratios of siRNA with late endosome/lysosome between TCMs and DCMs; Mander's coefficients of TCMs and DCMs were calculated to be 0.33 ± 0.12 and 0.50 ± 0.06 ($P > 0.05$), respectively, using Imaris software (Bitplane, Zurich, Switzerland).

We then assumed that siRNA release from the micelles within the cells might affect the gene silencing efficiency, because siRNA ultimately needs to be released and gain access to RNAi machinery in the cytoplasm. To investigate the release profile of siRNA, each micelle was prepared with both Alexa488-labeled siRNA and Alexa546-labeled siRNA (1:1 in molar ratio) to generate the FRET signal associated with the micelle formation [40]. Indeed, the excitation of Alexa488 allowed the adjacent Alexa546 within the micelle to emit the fluorescence via FRET, whereas the simple mixture of naked siRNAs did not show such a FRET signal (Fig. S6). The FRET pair-loaded TCMs or DCMs were incubated with HeLa-Luc cells and their FRET signal within the cells was observed by CLSM via the excitation at 488 nm. The FRET efficiency (Alexa546 intensity/Alexa488 intensity) in each pixel was calculated and expressed in a rainbow scale, where blue, green, and red indicate low, moderate,

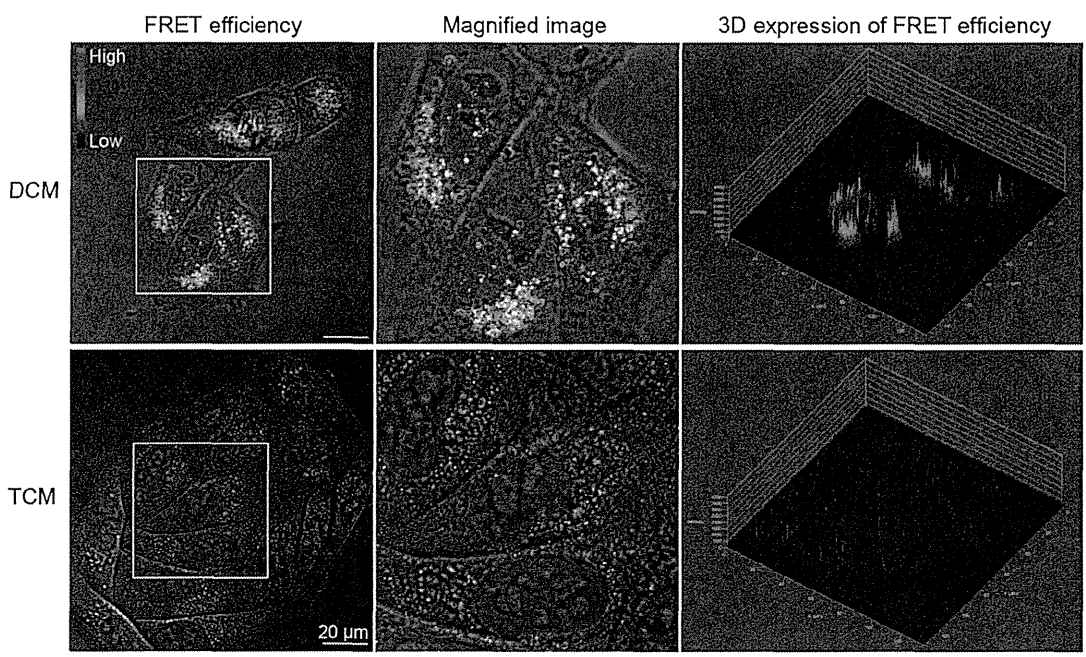

Fig. 6. FRET images of the micelles within cultured HeLa-Luc cells 12 h after the start of image acquisition. FRET ratio (Alexa546 intensity/Alexa488 intensity × 500) was calculated and expressed in a rainbow scale, where red, green, and blue signals mean high, moderate, and low FRET efficiency, respectively. The magnified images in the middle row correspond to the white squares in the left images. In the right row, the FRET efficiency was expressed in z-axis.

and high FRET efficiency, respectively (Fig. 6 and Movies S1–S2). The DCMs showed distinct red and green pixels, compared to TCMs, and maintained their higher FRET efficiency at least for 12 h. Considering that DCMs and TCMs showed similar FRET ratio in an aqueous solution as shown in Fig. S6, it is reasonable to conclude that DCMs did not effectively release siRNA in the cells, compared to TCMs. This ineffective release of siRNA might be explained by irreversible aggregate formation of DCMs in the serum-containing medium, as demonstrated in the FCS study (Fig. 3). In contrast, the cells treated with TCMs displayed more widely spreading and much lower FRET signals in the cell interior. Considering the result obtained from the intracellular trafficking study (Fig. S5), it is concluded that a major portion of the uptaken TCMs efficiently released siRNA payloads after endocytosis, whereas entrapped in late endosome/lysosome. It should be further noted that a minor portion of the released siRNAs should be located in the cytoplasm, as indicated by the significant gene silencing activity of TCMs (Fig. 4A). Note that a possible mechanism of the endosomal escape of TCMs is the endosomal membrane destabilization induced by direct interactions between the endosomal membrane and the hydrophobized polycationic chains released from TCMs [15,20]. The smooth release of siRNA from TCMs within the cells is presumably due to the result that PEG shell should avoid the aggregate formation inside the cells as well as in the serum-containing medium. Therefore, the higher gene silencing activity of TCMs might be explained by their balanced stability for enduring in the cell culture medium and then releasing siRNA within the cells.

Supplementary video related to this article can be found at http://dx.doi.org/10.1016/j.biomaterials.2014.02.016

4. Conclusion

In this study, an A-B-C type of triblock copolymer, PEG-PLys-PAsp(DET-DN), was synthesized for construction of three-layered polymeric micelles featuring hydrophobic core, siRNA-loaded intermediate layer, and PEG shell. The triblock copolymer self-assembled into uniform and spherical micellar architectures having a hydrodynamic diameter of sub-100 nm, associated with a hydrophobic core having a size of ~20 nm. The resulting TCMs stably encapsulated siRNA in the biological medium without dissociation and aggregation, presumably due to the PAsp(DET-DN) core and PEG shell. Consequently, the TCMs achieved efficient sequence-specific gene silencing in cultured HeLa-Luc cells without cytotoxicity. The comparative studies of TCMs with control micelles (RCMs and DCMs) revealed that their greater gene silencing activity should be due to both the efficient cellular uptake and the smooth release of siRNA inside the cells. These results demonstrate that the sophisticated arrangement of functional segments in triblock copolymer expands the performance of polymeric micelles for successful siRNA delivery. The present formulation of TCMs can be further developed toward the stimuli-responsive siRNA delivery based on the DN moiety.

Acknowledgment

This work was supported by the Funding Program for World-Leading Innovative R&D on Science and Technology (FIRST Program) from the Japan Society for the Promotion of Science (JSPS), Grant-in-Aid for Scientific Research from the Japanese Ministry of Education, Culture, Sports, Science and Technology.

Appendix A. Supplementary data

Supplementary data related to this article can be found at http://dx.doi.org/10.1016/j.biomaterials.2014.02.016.

References

[1] Aagaard L, Rossi JJ. RNAi therapeutics: principles, prospects and challenges. Adv Drug Deliv Rev 2007;59:75–86.
[2] Whitehead KA, Langer R, Anderson DG. Knocking down barriers: advances in siRNA delivery. Nat Rev Drug Discov 2009;8:129–38.
[3] Wagner E. Polymers for siRNA delivery: inspired by viruses to be targeted, dynamic, and precise. Acc Chem Res 2012;45:1005–13.
[4] Kataoka K, Harada A, Nagasaki Y. Block copolymer micelles for drug delivery: design, characterization and biological significance. Adv Drug Deliv Rev 2001;47:113–31.
[5] Kakizawa Y, Kataoka K. Block copolymer micelles for delivery of gene and related compounds. Adv Drug Deliv Rev 2002;54:203–22.
[6] Christie RJ, Nishiyama N, Kataoka K. Delivering the code: polyplex carriers for deoxyribonucleic acid and ribonucleic acid interference therapies. Endocrinology 2010;151:466–73.
[7] Matsumura Y, Maeda H. A new concept for macromolecular therapeutics in cancer chemotherapy: mechanism of tumoritropic accumulation of proteins and the antitumor agent smancs. Cancer Res 1986;46:6387–92.
[8] Maeda H. Macromolecular therapeutics in cancer treatment: the EPR effect and beyond. J Control Release 2012;164:138–44.
[9] Cabral H, Matsumoto Y, Mizuno K, Chen Q, Murakami M, Kimura M, et al. Accumulation of sub-100 nm polymeric micelles in poorly permeable tumours depends on size. Nat Nanotechnol 2011;6:815–23.
[10] Kakizawa Y, Harada A, Kataoka K. Environment-sensitive stabilization of core-shell structured polyion complex micelle by reversible cross-linking of the core through disulfide bond. J Am Chem Soc 1999;121:11247–8.
[11] Miyata K, Kakizawa Y, Nishiyama N, Harada A, Yamasaki Y, Koyama H, et al. Block catiomer polyplexes with regulated densities of charge and disulfide cross-linking directed to enhance gene expression. J Am Chem Soc 2004;126:2355–61.
[12] Christie RJ, Matsumoto Y, Miyata K, Nomoto T, Fukushima S, Osada K, et al. Targeted polymeric micelles for siRNA treatment of experimental cancer by intravenous injection. ACS Nano 2012;6:5174–89.
[13] Wang Y, Gao S, Ye WH, Yoon HS, Yang YY. Co-delivery of drugs and DNA from cationic core-shell nanoparticles self-assembled from a biodegradable copolymer. Nat Mater 2006;5:791–6.
[14] Kim WJ, Christensen LV, Jo S, Yockman JW, Jeong JH, Kim YH, et al. Cholesteryl oligoarginine delivering vascular endothelial growth factor siRNA effectively inhibits tumor growth in colon adenocarcinoma. Mol Ther 2006;14:343–50.
[15] Oba M, Miyata K, Osada K, Christie RJ, Sanjoh M, Li W, et al. Polyplex micelles prepared from ω-cholesteryl PEG-polycation block copolymers for systemic gene delivery. Biomaterials 2011;32:652–63.
[16] Kim HJ, Ishii T, Zheng M, Watanabe S, Toh K, Matsumoto Y, et al. Multifunctional polyion complex micelle featuring enhanced stability, targetability, and endosome escapability for systemic siRNA delivery to subcutaneous model of lung cancer. Drug Deliv Transl Res 2014;4:50–60.
[17] Alshamsan A, Haddadi A, Incani V, Samuel J, Lavasanifar A, Uludag H. Formulation and delivery of siRNA by oleic acid and stearic acid modified polyethylenimine. Mol Pharmacol 2009;6:121–33.
[18] Kim HJ, Ishii A, Miyata K, Lee Y, Wu S, Oba M, et al. Introduction of stearoyl moieties into a biocompatible cationic polyaspartamide derivative, PAsp(-DET), with endosomal escaping function for enhanced siRNA-mediated gene knockdown. J Control Release 2010;145:141–8.
[19] Oskuee RK, Philipp A, Dehshahri A, Wagner E, Ramezani M. The impact of carboxyalkylation of branched polyethylenimine on effectiveness in small interfering RNA delivery. J Gene Med 2010;12:729–38.
[20] Kim HJ, Oba M, Pittella F, Nomoto T, Cabral H, Matsumoto Y, et al. PEG-detachable cationic polyaspartamide derivatives bearing stearoyl moieties for systemic siRNA delivery toward subcutaneous BxPC3 pancreatic tumor. J Drug Target 2012;20:33–42.
[21] Kim D, Hong J, Moon H, Nam HY, Mok H, Jeong JH, et al. Anti-apoptotic cardioprotective effects of SHP-1 gene silencing against ischemia-reperfusion injury: use of deoxycholic acid-modified low molecular weight polyethyleneimine as a cardiac siRNA-carrier. J Control Release 2013;168:125–213.
[22] Mya KY, Lin EMJ, Gudipati CS, Gose HB, He C. Self-assembly of block copolymer micelles: synthesis via reversible addition-fragmentation chain transfer polymerization and aqueous solution properties. J Phys Chem B 2010;114:9128–34.
[23] Moughton AO, Hillmyer MA, Lodge TP. Multicompartment block polymer micelles. Macromolecules 2012;45:2–19.
[24] Bates FS, Hillmyer MA, Lodge TP, Bates CM, Delaney KT, Fredrickson GH. Multiblock polymers: panacea or pandora's box? Science 2012;336:434–40.
[25] Harada A, Cammas S, Kataoka K. Stabilized α-helix structure of poly(L-lysine)-block-poly(ethylene glycol) in aqueous medium through supramolecular assembly. Macromolecules 1996;29:6183–8.
[26] Miyata K, Fukushima S, Nishiyama N, Yamasaki Y, Kataoka K. PEG-based block catiomers possessing DNA anchoring and endosomal escaping functions to form polyplex micelles with improved stability and high transfection efficacy. J Control Release 2007;122:252–60.
[27] Shimizu H, Hori Y, Kaname S, Yamada K, Nishiyama N, Matsumoto S, et al. siRNA-based therapy ameliorates glomerulonephritis. J Am Soc Nephrol 2010;21:622–33.

[28] Buyens K, Meyer M, Wagner E, Demeester J, De Smedt SC, Sanders NN. Monitoring the disassembly of siRNA polyplexes in serum is crucial for predicting their biological efficacy. J Control Release 2010;141:38–41.
[29] Nakanishi M, Park JS, Jang WD, Oba M, Kataoka K. Study of the quantitative aminolysis reaction of poly(β-benzyl L-aspartate) (PBLA) as a platform polymer for functionality materials. React Funct Polym 2007;67:1361–72.
[30] Oba M, Fukushima S, Kanayama N, Aoyagi K, Nishiyama N, Koyama H, et al. Cyclic RGD peptide-conjugated polyplex micelles as a targetable gene delivery system directed to cells possessing $\alpha_v\beta_3$ and $\alpha_v\beta_5$ integrins. Bioconjug Chem 2007;18:1415–23.
[31] Zhao H, Sterner ES, Coughlin EB, Theato P. o-Nitrobenzyl alcohol derivatives: opportunities in polymer and materials science. Macromolecules 2012;45:1723–36.
[32] Miguel VS, Bochet CG, Compo A. Wavelength-selective caged surfaces: how many functional levels are possible? J Am Chem Soc 2011;133:5380–8.
[33] Harris JR, Roos C, Djalali R, Rheingans O, Maskos M, Schmidt M. Application of the negative staining technique to both aqueous and organic solvent solutions of polymer particles. Micron 1999;30:289–98.
[34] Zhulina EB, Borisov OV. Theory of block polymer micelles: recent advances and current challenges. Macromolecules 2012;45:4429–40.
[35] Fukushima S, Miyata K, Nishiyama N, Kanayama N, Yamasaki Y, Kataoka K. PEGylated polyplex micelles from triblock cationers with spatially ordered layering of condensed pDNA and buffering units for enhanced intracellular gene delivery. J Am Chem Soc 2005;127:2810–1.
[36] Miyata K, Oba M, Kano MR, Fukushima S, Vachutinsky Y, Han M, et al. Polyplex micelles from triblock copolymers composed of tandemly aligned segments with biocompatible, endosomal escaping, and DNA-condensing functions for systemic gene delivery to pancreatic tumor. Pharm Res 2008;25:2924–36.
[37] Xu X, Smith AE, Kirkland SE, McCormick CL. Aqueous RAFT synthesis of pH-responsive triblock copolymer mPEO-PAPMA-PDPAEMA and formation of shell cross-linked micelles. Macromolecules 2008;41:8429–35.
[38] Jiang X, Zhang G, Narain R, Liu S. Fabrication of two types of shell-cross-linked micelles with "inverted" structures in aqueous solution from schizophrenic water-soluble ABC triblock copolymer via click chemistry. Langmuir 2009;25:2046–54.
[39] Itaka K, Kataoka K. Recent development of nonviral gene delivery systems with virus-like structures and mechanisms. Eur J Pharm Biopharm 2009;71:475–83.
[40] Chen H, Kim S, Li L, Wang S, Park K, Cheng JX. Release of hydrophobic molecules from polymer micelles into cell membranes revealed by Forster resonance energy transfer imaging. Proc Natl Acad Sci U S A 2008;105:6596–601.

nature COMMUNICATIONS

ARTICLE

Received 23 Nov 2013 | Accepted 3 Mar 2014 | Published 2 Apr 2014

DOI: 10.1038/ncomms4545

Three-layered polyplex micelle as a multifunctional nanocarrier platform for light-induced systemic gene transfer

Takahiro Nomoto[1], Shigeto Fukushima[2], Michiaki Kumagai[2], Kaori Machitani[2], Arnida[2], Yu Matsumoto[3], Makoto Oba[4], Kanjiro Miyata[3], Kensuke Osada[1,5], Nobuhiro Nishiyama[6] & Kazunori Kataoka[1,2,3]

Nanocarriers responding to light have great potential for pinpoint therapy, and recent studies have revealed promising *in vivo* activity. However, light-selective gene transfer still remains challenging in the systemic application. Here we report systemic light-responsive nanocarriers for gene delivery developed through the sequential self-assembly of ABC-type triblock copolymer/DNA/dendrimeric photosensitizer, forming polyplex micelles with three-layered functional nanocompartments. The DNA-packaged core is covered by the photosensitizer-incorporated intermediate layer, which is encompassed by an outer shielding shell. This three-layered structure permits multistep photosensitizer and DNA delivery into a solid tumour by a systemic route: the shielding layer minimizes unfavourable interactions with blood components, and the photosensitizer is delivered to endo-/lysosomal membranes to facilitate light-selective cytoplasmic translocation of the micelles, accomplishing DNA delivery into the nucleus to exert gene expression. The polyplex micelles display >100-fold photoenhanced gene expression in cultured cells and exhibit light-induced *in vivo* gene transfer in solid tumours following systemic administration.

[1] Department of Bioengineering, Graduate School of Engineering, The University of Tokyo, 7-3-1 Hongo, Bunkyo-ku, Tokyo 113-8656, Japan. [2] Department of Materials Engineering, Graduate School of Engineering, The University of Tokyo, 7-3-1 Hongo, Bunkyo-ku, Tokyo 113-8656, Japan. [3] Center for Disease Biology and Integrative Medicine, Graduate School of Medicine, The University of Tokyo, 7-3-1 Hongo, Bunkyo-ku, Tokyo 113-0033, Japan. [4] Graduate School of Biomedical Sciences, Nagasaki University, 1-14 Bunkyo-machi, Nagasaki 852-8521, Japan. [5] Precursory Research for Embryonic Science and Technology (PRESTO), Japan Science and Technology Agency (JST), 4-1-8 Honcho, Kawaguchi, Saitama 332-0012, Japan. [6] Polymer Chemistry Division, Chemical Resources Laboratory, Tokyo Institute of Technology, R1-11, 4259 Nagatsuta, Midori-ku, Yokohama 226-8503, Japan. Correspondence and requests for materials should be addressed to N.N. (email: nishiyama@res.titech.ac.jp) or to K.K. (email: kataoka@bmw.t.u-tokyo.ac.jp).

Nanocarriers are aimed at delivering bioactive substances to target sites and eliciting their biological functions in a spatiotemporally controlled manner, thereby achieving enhanced therapeutic efficacy with minimal side effects[1–5]. These carriers need to achieve selective extravasation at target tissues after systemic administration, and a mechanism to circumvent intracellular barriers, such as effective transport from endosomal compartments to the cytoplasm, is indispensable for efficacy, particularly for gene and oligonucleotide delivery[6].

Physical energy in the form of light, ultrasound or magnetism can be used as a spatiotemporally controllable trigger to facilitate the overcoming of such biological barriers by nanocarriers[7–9]. Owing to recent advances in laser technology, light has become a useful and safe energy source, and laser therapy and photodynamic therapy are in practical use[10–12]. More recently, enhanced cytoplasmic delivery of macromolecular compounds by photochemical disruption of the endo-/lysosomal membrane, termed photochemical internalization (PCI), has attracted much attention[13–16]. Although PCI has been proven to work for gene transduction in cultured cells and epithelial tissues by local administration, this concept has yet to succeed *in vivo* in systemic applications. The greatest challenge in systemic PCI-mediated gene transduction is the simultaneous delivery of the gene (plasmid DNA; pDNA) and the photosensitizer (PS) to the target cell. Hence, nanocarriers need to incorporate both the pDNA and the PS; however, these molecules should be compartmentalized because a PS may inactivate pDNA through the formation of reactive oxygen species (ROS). In addition, nanocarriers should possess a shielding surface to avoid undesirable interactions with biological components.

Here we report the first success in *in vivo* PCI-mediated gene transduction by systemic administration of a multi-compartmentalized nanocarrier newly designed for this purpose, as shown in Fig. 1. The key to forming spatially segregated, three-layered compartments within a single nanocarrier platform is the sequential self-assembly of pDNA and dendrimeric PS (DPc) with triblock copolymers composed of tandemly aligned segments with distinct functionality in an aqueous solution. The nanocarrier thus has a core compartment for stable packaging of pDNA, an intermediate compartment for incorporation of DPc to induce PCI, and an outer hydrophilic compartment of poly(ethylene glycol) (PEG) that forms a shielding surface. The three-layered nanocarrier, termed DPc-TPM (a DPc-loaded ternary polyplex micelle), accommodates DPc and pDNA in these segregated compartments, thereby preventing photochemical damage to the encapsulated pDNA. Furthermore, integrated carboxylate groups on the periphery of the DPc contribute to its stable disposition in the intermediate cationic compartment. In turn, the acidic compartment of the endo-/lysosome neutralizes these carboxylate groups to facilitate the translocation of the amphiphilic DPc from the micellar compartment into the endo-/lysosomal membrane, thereby inducing a strong PCI effect. Consequently, using this DPc-TPM, successful PCI-mediated gene transduction through the systemic route is demonstrated in a xenografted tumour model in mice.

Results

Construction and characterization of DPc-TPMs. First, pDNA and PEG-poly{*N*-[*N*-(2-aminoethyl)-2-aminoethyl]aspartamide}-poly(L-lysine) (PEG-PAsp(DET)-PLys; PEG: 12,000 ($g\,mol^{-1}$), degree of polymerization (DP) of PAsp(DET): 34, DP of PLys: 52) were mixed at the stoichiometric charge ratio of PLys and pDNA ((amino groups in PLys)/(phosphate groups in pDNA); Lys/pDNA = 1) to form pDNA/PEG-PAsp(DET)-PLys polyplex micelles. PLys has higher binding affinity to pDNA than PAsp(DET)[17,18]; therefore, the PLys segment in the block copolymer selectively interacts with pDNA under this condition to form the three-layered polyplex micelle consisting of a PLys/pDNA polyplex core, a PAsp(DET) intermediate compartment and a PEG shell, as confirmed by ^{1}H NMR (proton nuclear magnetic resonance) measurement (Supplementary Fig. 1).

DPc with 32 carboxyl groups at the periphery (see the DPc chemical structure and absorption spectrum presented in Fig. 1b and Supplementary Fig. 2, respectively) was then incorporated into the PAsp(DET) intermediate compartment through electrostatic interaction to create DPc-TPM for light-selective transfection. DPc was integrated into the three-layered polyplex micelles by simple mixing at various molar ratios of peripheral carboxyl groups on DPc to the protonated amino groups on PAsp(DET) (DPc/Asp(DET) ratios). Note that the side-chain diaminoethane units of PAsp(DET) are not completely protonated at pH 7.3 (these units are approximately in the single protonated state, according to a previously reported titration result)[19]. The simultaneous incorporation of pDNA and DPc into the micelles was confirmed by gel retardation assay and ultracentrifugation (Supplementary Figs 3 and 4). The gel retardation assay revealed complete pDNA incorporation into the micelle at the DPc/Asp(DET) ratio of 0–4 (Supplementary Fig. 3). At DPc/Asp(DET) ratios >4.5, appreciable release of pDNA from the micelles was observed, suggesting the replacement of pDNA by excess DPc. The ultracentrifugation study provided quantitative information on micelle composition (Supplementary Fig. 4). At the DPc/Asp(DET) ratio of 1 (charge stoichiometric ratio), almost all DPc (98%) was incorporated into micelles. Interestingly, the proportional incorporation of DPc into micelles was observed even under an excess charge ratio of DPc to PAsp(DET) (DPc/Asp(DET) ratio of 2–4). Because DPc is known to induce secondary aggregation at higher concentrations in aqueous solution owing to hydrophobic interactions, even at pH 7.4 (ref. 20), DPc deposited within the PAsp(DET) compartment may facilitate further inclusion of DPc molecules above the stoichiometric charge ratio. Indeed, as the DPc/Asp(DET) ratio increased over the charge stoichiometry, the zeta potentials of the micelles were accordingly shifted to negative values (Supplementary Fig. 5), which is consistent with DPc inclusion beyond the charge stoichiometry.

The size and morphology of the three-layered polyplex micelles and the DPc-TPM were evaluated by transmission electron microscopy (TEM) after pDNA staining with uranyl acetate (Fig. 2a–d). The polyplex micelles (without DPc) exhibited characteristic rod-shaped structures (Fig. 2a). We also observed micelle shrinkage with a significant decrease in the major rod axis length through complex formation with DPc at a DPc/Asp(DET) ratio of 1 (Fig. 2b and e). The major rod axis length increased with further increases in the DPc/Asp(DET) ratio to 2 and 3 (Fig. 2c–e) as illustrated in Fig. 2f. This tendency towards morphological change was consistent with dynamic light scattering measurements (Supplementary Figs 6–8), which showed a smaller cumulant diameter and a lower polydispersity index at the DPc/Asp(DET) ratio of 1.

To gain further insight into the physicochemical properties of the DPc-TPM, the condensation level of pDNA in the polyplex was estimated by fluorescence resonance energy transfer (FRET). Here, pDNA was simultaneously labelled with fluorescein and Cy3. In the free form, fluorescein-Cy3-labelled pDNA emits efficient fluorescein fluorescence when excited at 470 ± 10 nm. Upon pDNA condensation by a polycation, fluorescein-Cy3-labelled pDNA emits Cy3 fluorescence owing to FRET between fluorescein and Cy3. Hence, FRET efficiency indicates the pDNA condensation state[21,22]. We measured the FRET efficiency of DPc-TPM using different amounts of fed DPc. We also examined

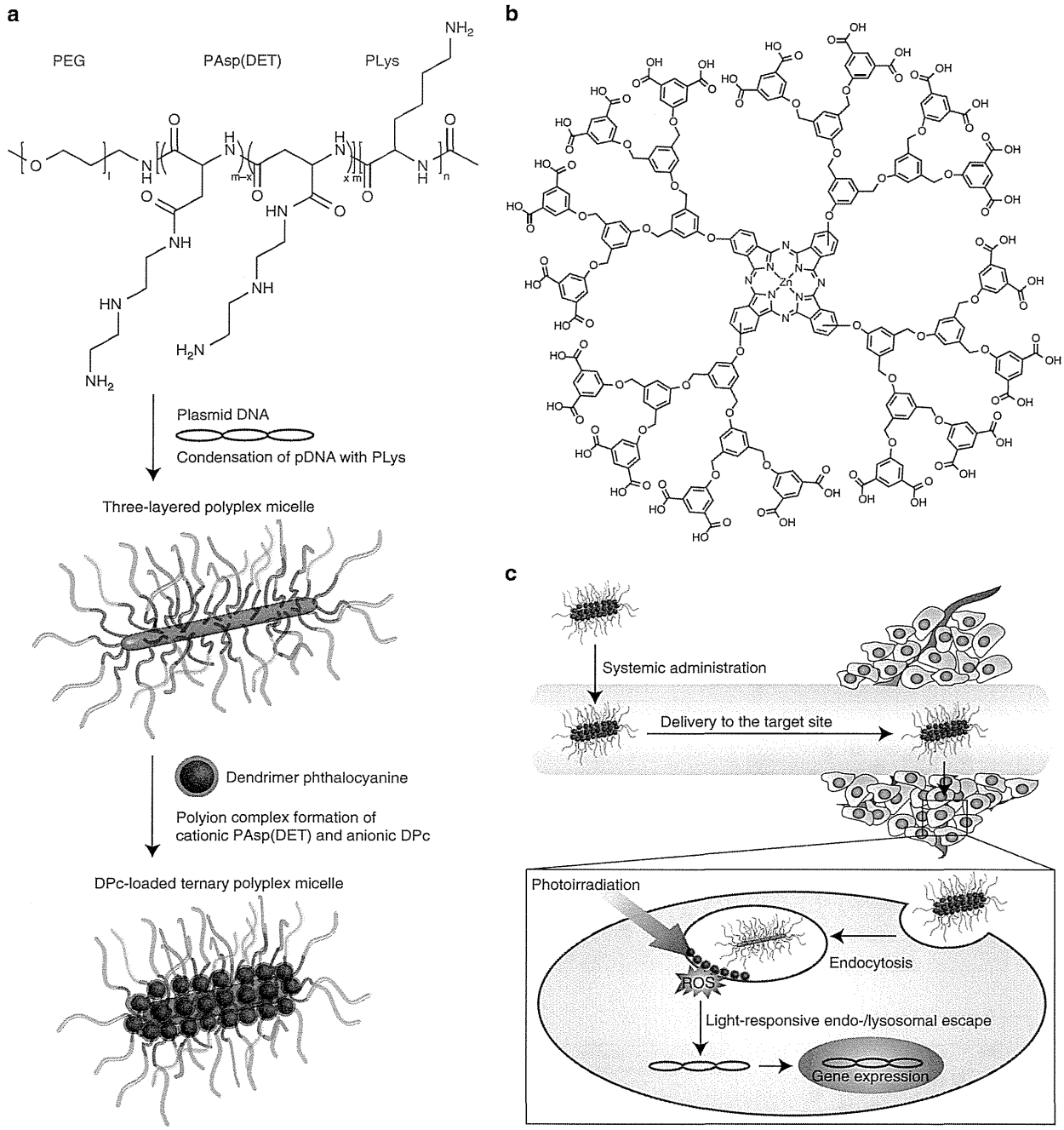

Figure 1 | Construction of the DPc-TPM and light-responsive gene transfer. (**a**) Design of the DPc-TPM. First, a three-layered polyplex micelle is prepared by mixing PEG-PAsp(DET)-PLys triblock copolymer and pDNA; the polyplex micelle is composed of a PEG shell, an intermediate PAsp(DET) layer and a PLys/pDNA core. The DPc-TPM is constructed by adding DPc to the PAsp(DET) intermediate layer. (**b**) Chemical structure of DPc. (**c**) Scheme showing the delivery at systemic and intracellular levels. At the systemic level, DPc-TPM circulates in the bloodstream; non-specific interaction with biological components is prevented after intravenous injection. In the target tissue (a solid tumour), DPc-TPMs are taken up by cells via endocytosis and entrapped in endo-/lysosomes. In response to the low pH prevalent in the endo-/lysosome, DPc is released from the DPc-TPMs owing to the protonation of the peripheral carboxyl groups and interacts with the endo-/lysosomal membrane through hydrophobic interactions. Upon photoirradiation, DPc generates ROS that destabilize the endo-/lysosomal membrane, facilitating endo-/lysosomal escape.

FRET efficiency in two other polyplexes as controls. One control was a randomly mixed TPM (random-TPM), which was prepared by randomly mixing pDNA, DPc and PEG-PAsp(DET)-PLys. The other control was a TPM without the intermediate layer (diblock-TPM), which was prepared by adding DPc to a pDNA/PEG-PLys polyplex micelle (PEG: 12,000 ($g\,mol^{-1}$), DP of PLys: 45, Lys/pDNA = 1.5) having no intermediate compartment. The preparation of these polyplexes is illustrated in Fig. 3a–c. FRET efficiency was defined as the ratio of fluorescein intensity to Cy3 fluorescence intensity (fluorescein/Cy3) and is summarized in Fig. 3d. In the absence of DPc, all micelles exhibited similar fluorescein/Cy3, indicating similar states of pDNA condensation.

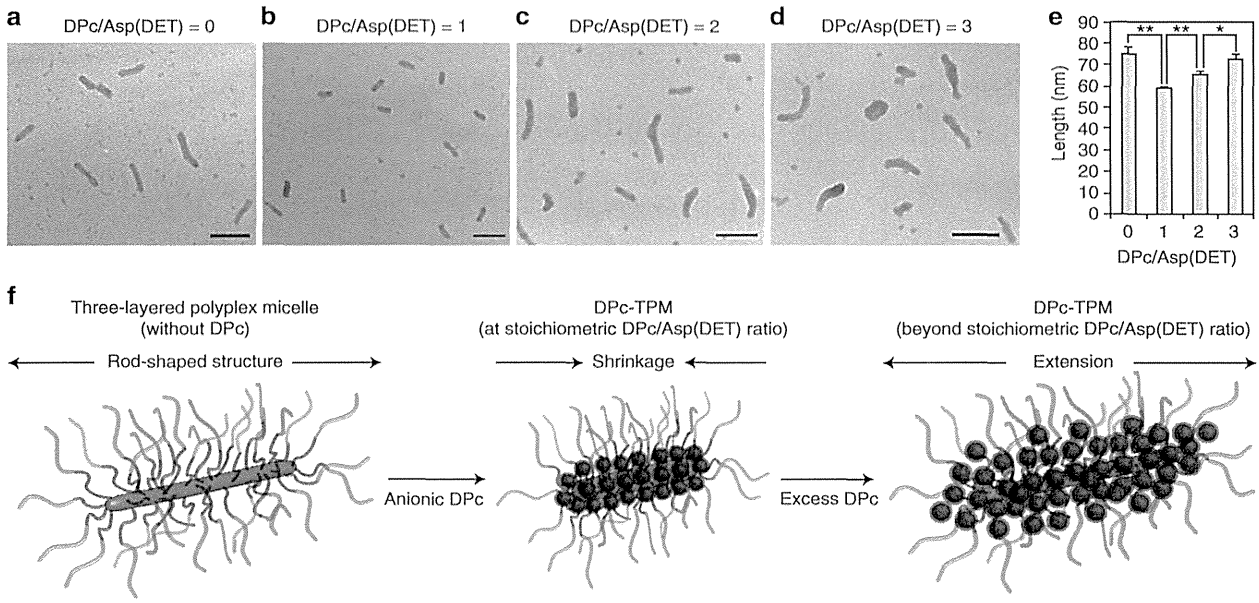

Figure 2 | TEM images of three-layered polyplex micelles and DPc-TPMs. (**a**–**d**) The morphology of the three-layered polyplex micelles and the DPc-TPMs was observed using TEM at 50,000-fold magnification: (**a**) pDNA/PEG-PAsp(DET)-PLys polyplex micelles (DPc/Asp(DET) = 0); (**b**–**d**) DPc-TPMs (DPc/Asp(DET) = 1–3). pDNA was visualized by staining with uranyl acetate. Scale bars, 100 nm. (**e**) The major axis length of the packaged pDNA within the polyplex micelles was measured based on the TEM images. The results are expressed as means ± s.e.m. ($n = 100$). $^{*}P < 0.05$, $^{**}P < 0.01$ (*t*-test). (**f**) A schematic diagram used to explain the results shown in **a**–**e**.

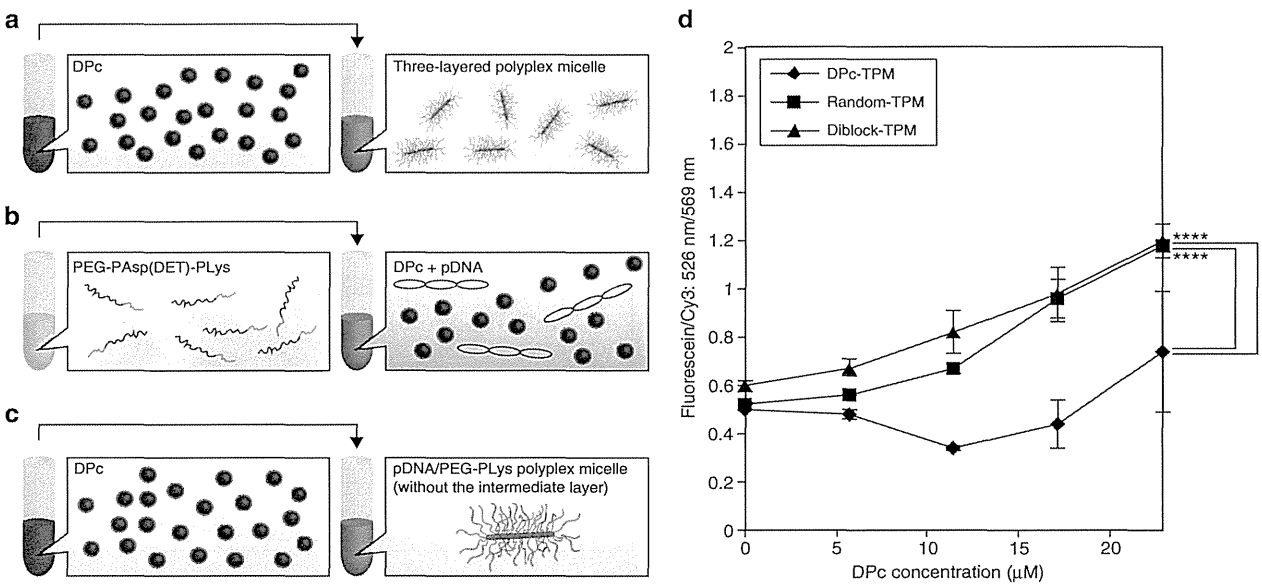

Figure 3 | The effect of DPc concentration on pDNA condensation. (**a**–**c**) The preparation of (**a**) DPc-TPMs, (**b**) random-TPMs, and (**c**) diblock-TPMs. (**d**) FRET induced by the condensation of pDNA labelled with fluorescein and Cy3. Fluorescein/Cy3 (fluorescence intensity at 526 nm/fluorescence intensity at 569 nm) of DPc-TPMs, random-TPMs and diblock-TPMs was calculated as a FRET indicator and plotted against DPc concentration. The DPc concentration of 5.7 μM is equivalent to a DPc/Asp(DET) ratio of 1 in DPc-TPMs. The results are expressed as means ± s.e.m. ($n = 3$). $^{****}P < 0.0001$ (two-way analysis of variance using the Tukey–Kramer test).

For the two control samples, an increase in DPc concentration led to marked enhancement in fluorescein/Cy3, indicating decreased FRET efficiency. This result is reasonably explained by a scheme in which DPc interaction attenuates pDNA condensation. By contrast, the DPc-TPMs did not exhibit any increase in fluorescein/Cy3 from the original value. This result is consistent with the three-layered structure of the DPc-TPM in which pDNA is well segregated from the PAsp(DET) layer through selective complexation with PLys, eventually maintaining the integrity of the condensed state even in the presence of anionically charged DPc.

ROS generated by photoirradiated PS may damage nearby pDNA. We assume that compartmentalizing and segregating pDNA and DPc in the DPc-TPM reduces photochemical damage to pDNA. In this study, we photoirradiated DPc-TPMs (DPc/Asp(DET) = 2) and random-TPMs (DPc/Asp(DET) = 2) using a

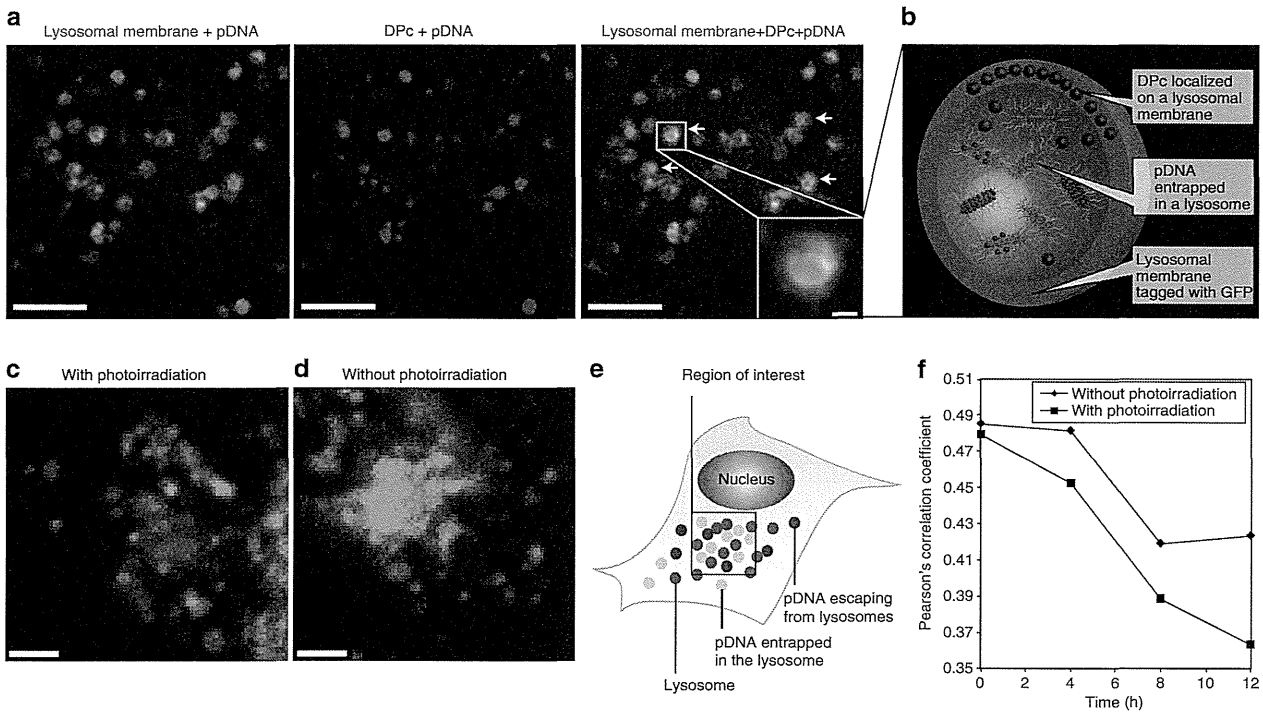

Figure 4 | The subcellular distribution of DPc-TPMs. (**a**) Super-resolution microscopic imaging of GFP-lysosomal membranes (green), Cy3-labelled pDNA (red) and DPc (blue). HeLa cells were incubated with DPc-TPMs (DPc/Asp(DET) = 1) for 6 h and then fixed. White arrows indicate the colocalization of lysosomal membranes and DPc. Original magnification, × 100. Before selecting this representative image, 18 images (47.58 μm × 47.48 μm (1,904 pixels × 1,900 pixels) × 18 images) were studied. Scale bar, 2 μm (magnified image, 200 nm). (**b**) Schematic view of the assumed localization of DPc and pDNA in the lysosomal compartment. (**c**) Confocal imaging of the subcellular distribution of the micelles 15.5 h after photoirradiation. HeLa cells were incubated with DPc-TPMs for 6 h, followed by medium replacement and photoirradiation at a fluence of 2 J cm^{-2}. The image was captured 15.5 h after photoirradiation. Lysosomal membranes were tagged with GFP (green). Cy3-labelled pDNA is shown in red. Original magnification, × 63. This representative image was selected from nine images (134.82 μm × 134.82 μm (1,024 pixels × 1,024 pixels) × 9 images). Scale bar, 2 μm. (**d**) Confocal imaging of the subcellular distribution of DPc-TPMs without photoirradiation. HeLa cells were incubated with DPc-TPMs at the DPc/Asp(DET) ratio of 1 for 6 h, followed by medium replacement. The image was captured 15.5 h after medium replacement. Original magnification, × 63. This representative image was selected from nine images (134.82 μm × 134.82 μm (1,024 pixels × 1,024 pixels) × 9 images). Scale bar, 2 μm. (**e**) A schematic diagram used to explain the results shown in **c**,**d**. (**f**) Quantification of Pearson's correlation coefficient between lysosomes-GFP and Cy3-labelled pDNA. The indicated time point indicates the elapsed time after the start of the movie acquisition.

300-W halogen lamp (fluence rate, 3.0 mW cm^{-2}) equipped with a band filter (400–700 nm) and then quantified the amount of intact pDNA using electrophoresis (Supplementary Fig. 9). Without photoirradiation, pDNA remained intact in both cases as confirmed based on the SYBR Green I fluorescence intensities of supercoiled pDNA. Smeared pDNA bands were evident in both cases with photoirradiation. However, a higher fraction of intact supercoiled pDNA was observed in DPc-TPMs (69% and 49% of the original fluorescence intensity after photoirradiation with 2 J cm^{-2} and 4 J cm^{-2}, respectively) compared with that in random-TPMs (51% and 27% of the original fluorescence intensity after photoirradiation with 2 J cm^{-2} and 4 J cm^{-2}, respectively, under the same conditions). This result strongly suggests that the pDNA condensed in the inner core was successfully compartmentalized and segregated from the DPc-incorporated intermediate layer, thereby allowing pDNA to avoid oxidative damage by ROS produced by DPc.

***In vitro* activity of DPc-TPMs.** The internalization of DPc-TPMs into HeLa cells (cancerous cells) and HUVECs (human umbilical vein endothelial cells; normal cells) was evaluated using confocal laser scanning microscopy (CLSM) (Supplementary Fig. 10 and Supplementary Methods). Although the DPc-TPMs were internalized into both HeLa cells and HUVECs (Supplementary Fig. 10a,b), significantly higher cellular uptake was observed in HeLa cells than in HUVECs (Supplementary Fig. 10e). It is known that cancerous cells take up more circumjacent substances than normal cells, accounting for the difference in the cellular uptake.

Following cellular internalization, DPc-TPMs are expected to release DPc under acidic conditions in the endo-/lysosomes because the peripheral carboxyl groups of DPc undergo protonation at pH 5.5 (ref. 23). Simultaneously, DPc exhibiting increased hydrophobicity because of the protonation of peripheral carboxyl groups may interact with endo-/lysosomal membranes, which is critical for the light-induced endo-/lysosomal escape of DPc-TPMs (Fig. 1c). Subcellular distribution of DPc was observed in HeLa cells after 6 h of incubation with the polyplexes (DPc/Asp(DET) = 1) using super-resolution microscopy (structured illumination microscopy; this technique provides better spatial resolution than conventional light microscopy, thereby distinguishing between the lysosomal membrane and the interior of the lysosome more clearly) (Fig. 4a). Cy3-labelled pDNA (red) was found inside lysosomes, the membranes of which were visualized using Lamp1-green fluorescent protein (GFP) (green). DPc (blue) was localized on lysosomal membranes and in the lysosomes, indicating that DPc interacts with the lysosomal membranes, presumably after its

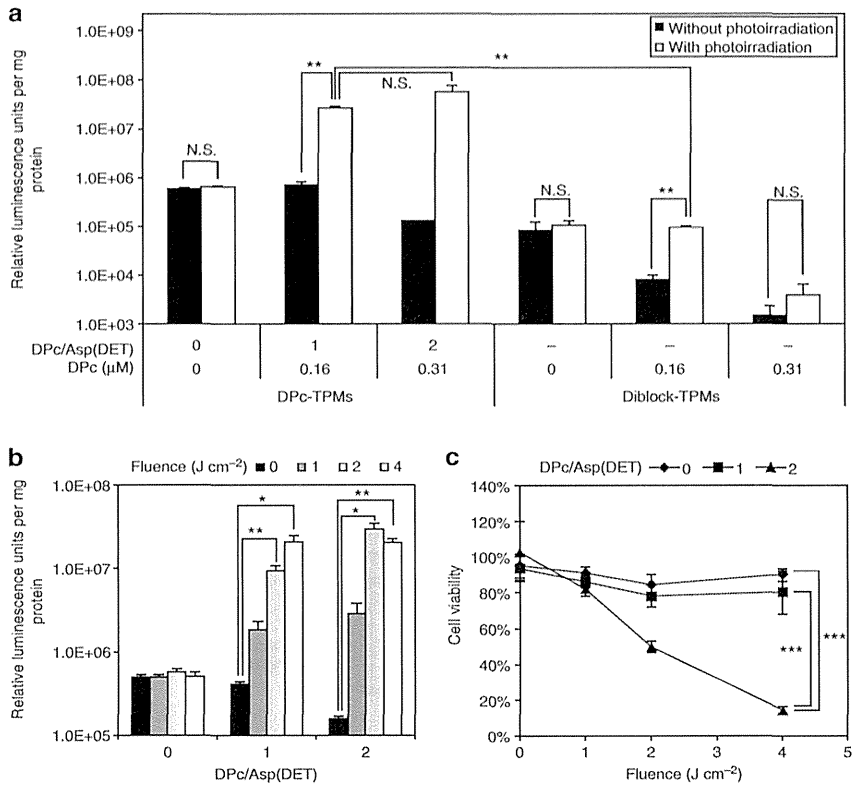

Figure 5 | *In vitro* transfection efficiency and cytotoxicity to HeLa cells. (**a**) The effect of photoirradiation on the transfection efficiency of DPc-TPMs and diblock-TPMs at DPc concentrations equivalent to DPc/Asp(DET) ratios of 0–2 in DPc-TPMs. Photoirradiation was performed 6 h after incubation with each sample, followed by 40 h post incubation in fresh medium and a subsequent luciferase assay. (**b**) The effect of photoirradiation fluence on the transfection efficiency of DPc-TPMs at various DPc/Asp(DET) ratios. The same experimental conditions as in **a** were applied. The results are expressed as means ± s.e.m. ($n = 4$). $^{*}P < 0.05$, $^{**}P < 0.01$ (*t*-test). (**c**) The cytotoxicity of DPc-TPMs. HeLa cells were incubated with DPc-TPMs for 6 h. The cells were washed with PBS and incubated in fresh medium, followed by photoirradiation with a fluence of 1, 2 or 4 J cm^{-2} and a further 40 h of incubation. For non-photoirradiated cells (0 J cm^{-2}), cells were incubated for 40 h in fresh medium after 6 h of incubation with DPc-TPMs and subsequent washing with PBS. Cell viability was then evaluated using an MTT assay. The results are expressed as means ± s.d. ($n = 8$ for 0 J cm^{-2} and $n = 4$ for 1, 2 and 4 J cm^{-2}). $^{***}P < 0.000001$ (two-way analysis of variance with the Fisher's least significant difference).

release from DPc-TPMs in the endo-/lysosomal compartments, as schematically shown in Fig. 4b.

Upon photoirradiation, DPc localized on lysosomal membranes is expected to disrupt the membrane structures via ROS production, leading to light-selective endo-/lysosomal escape of pDNA into the cytoplasm. This dynamic process was monitored using CLSM (Fig. 4c–e and Supplementary Movies 1–5). After 6 h of incubation with DPc-TPMs, HeLa cells were photoirradiated at a fluence of 2 J cm^{-2} (halogen lamp, 400–700 nm), and movie acquisition was started 3.5 h after photoirradiation. Initially, most Cy3-labelled pDNA was entrapped in lysosomes. However, 4 h later, some pDNA appeared to leak into the cytoplasm (Supplementary Movies 1–3). Twelve hours after the start of movie acquisition, pDNA became prominent outside the lysosomes, as seen from the clear red fluorescence in Fig. 4c and in Supplementary Movies 1–3. By contrast, without photoirradiation, such distinctive pDNA translocation was not observed (Fig. 4d and Supplementary Movies 4 and 5). We quantified the colocalization between the lysosomes and pDNA using Pearson's correlation coefficient (PCC) (Fig. 4f). At the start of data acquisition, the PCC value was 0.485 for the non-photoirradiated cells and 0.479 for the photoirradiated cells. The PCC value of the photoirradiated cells then steadily decreased and finally reached 0.363 at 12 h, whereas that of the non-photoirradiated cells only decreased to 0.423. These results are consistent with the PCI-mediated endo-/lysosomal escape of DPc-TPMs.

Light-induced endo-/lysosomal escape led to photoenhanced transfection of firefly luciferase (Fig. 5a). In the absence of DPc (DPc/Asp(DET) = 0), gene expression of the three-layered polyplex micelles was not altered by photoirradiation. However, DPc-TPMs at DPc/Asp(DET) ratios of 1 and 2 resulted in ~44- and 88-fold higher gene expression, respectively, than the polyplex micelle (DPc/Asp(DET) = 0), following photoirradiation. By contrast, diblock-TPMs (pDNA/PEG-PLys/DPc) exhibited apparently lower gene expression than DPc-TPMs, regardless of DPc and photoirradiation. DPc-TPMs also achieved photochemically enhanced gene transfer in HCT 116 cells (Supplementary Fig. 11 and Supplementary Methods). DPc-TPMs (DPc/Asp(DET) = 1 and 2) significantly increased gene expression in a light-induced manner, whereas diblock-TPMs did not accomplish such distinct photochemical enhancement. These results strongly suggest that the three-layered structure of DPc-TPM is critical for light-selective gene transfection.

The effects of photoirradiation fluence on light-induced transfection efficiency and photocytotoxicity in HeLa cells are shown in Fig. 5b and c, respectively. The three-layered polyplex micelle (DPc/Asp(DET) = 0) did not affect transfection activity and cytotoxicity upon photoirradiation. DPc-TPMs at DPc/Asp(DET) ratios of 1 and 2 displayed fluence-dependent

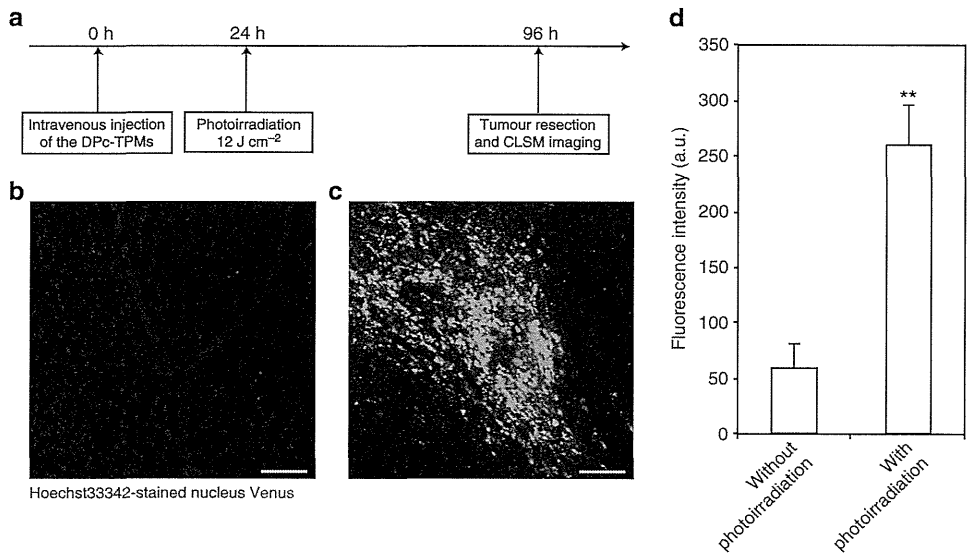

Figure 6 | *In vivo* transfection into a subcutaneous HeLa tumour model. (**a**) A scheme showing *in vivo* transfection. (**b**,**c**) *Ex vivo* CLSM images of the tumours (**b**) without photoirradiation and (**c**) with photoirradiation. A Hoechst 33342-stained nucleus and Venus fluorescence are shown in blue and green, respectively. Scale bars, 100 μm. (**d**) The Venus fluorescence intensity was quantified from the images after subtraction of the background intensity. The results are expressed as means ± s.e.m. ($n=5$ mice for tumours without photoirradiation and $n=6$ mice for tumours with photoirradiation). $^{**}P<0.01$ (*t*-test).

transfection efficiency, achieving >100-fold increases in light-selective transfection efficiency. With respect to photocytotoxicity, DPc-TPMs at a DPc/Asp(DET) ratio of 2 reduced cell viability with increased fluence. Excess DPc might photochemically damage organelles such as mitochondria or the endoplasmic reticulum after endo-/lysosomal escape[24]. However, DPc-TPMs at a DPc/Asp(DET) ratio of 1 achieved remarkable gene transfer in proportion to fluence without compromising cell viability. This non-cytotoxic PCI effect can be explained by multistep DPc and pDNA delivery: DPc delivery to the endo-/lysosomal membranes to modulate intracellular localization and pDNA delivery to the nucleus to exert gene expression (Fig. 1c).

***In vivo* activity of DPc-TPMs.** The potential of DPc-TPMs to act as light-responsive systemic gene nanocarriers was examined by transfecting a reporter gene (a variant of a yellow fluorescent protein, Venus) into a subcutaneous HeLa tumour in a mouse. We intravenously injected DPc-TPMs at the DPc/Asp(DET) ratio of 1 and photoirradiated the tumour with a semiconductor laser (680 nm, 12 J cm^{-2}) 24 h after systemic administration. The tumour was excised 3 days after photoirradiation, and Venus expression was observed using CLSM (Fig. 6). The non-photoirradiated tumour did not show distinct Venus expression (green) (Fig. 6b), whereas the photoirradiated tumour did show Venus expression (Fig. 6c). Venus fluorescence was quantified from the obtained CLSM images (Fig. 6d); the photoirradiated tumour exhibited ~4.4-fold higher fluorescence than the non-photoirradiated tumour. Interestingly, DPc-TPMs also accumulated in highly vascularized organs such as lung, liver, spleen and kidney, resulting in weak gene expression in those organs (Supplementary Fig. 12 and Supplementary Methods). However, Venus fluorescence intensity in these organs was significantly lower than that in the photoirradiated tumours ($P<0.01$ for lung, $P<0.01$ for liver and $P<0.05$ for kidney (*t*-test)). The selective gene expression in the tumour is consistent with the PCI function of DPc-TPMs, as demonstrated in Fig. 5, in which DPc-TPMs exerted distinct gene expression only in the presence of photoirradiation. We also confirmed PCI-mediated gene transfer after systemic administration using a subcutaneous HCT 116 tumour in a mouse (Supplementary Fig. 13 and Supplementary Methods). Photoirradiation (30 J cm^{-2}) to HCT 116 tumours 24 h after systemic administration of DPc-TPMs resulted in photochemically enhanced Venus expression. The photoirradiated tumour exhibited ~6.0-fold higher Venus fluorescence than the non-photoirradiated tumour. To our knowledge, these experiments are the first successful demonstrations of PCI-mediated gene transfection after systemic administration.

Discussion

Previous studies have revealed the validity of PCI as a method for the cytoplasmic delivery of anticancer drugs, genes, small interfering RNAs and immunotoxins[13–16,25–27]. PCI is notably successful in anticancer drug delivery; the use of PCI in combination with bleomycin is now in phase II clinical studies. However, *in vivo* application of PCI with nucleic acid compounds, including pDNA, has remained limited because the development of nanocarriers is a prerequisite for their delivery. We previously developed a light-responsive nanocarrier and succeeded in light-selective gene transfection after local administration[23]; however, the nanocarrier could be further improved for use in systemic applications. In this context, polymeric micellar structures offer great potential for systemic applications because polymeric micelles have been widely studied as systemically injectable nanocarrier platforms, and their therapeutic efficacy has been demonstrated[28–33]. The core compartment encapsulates therapeutic pDNA and protects it from enzymatic degradation; the shell compartment inhibits unfavourable interactions with biological components, yielding prolonged circulation times. Owing to these characteristics, the polyplex micelles can accumulate within highly vascularized tumours and exert therapeutic efficacy. In this study, to mount PCI function into the polyplex micelle, we synthesized PEG-PAsp(DET)-PLys, thereby enabling the construction of DPc-TPMs containing an intermediate layer encapsulating DPc to achieve systemic light-selective gene transfer.

In DPc-TPMs, pDNA exhibited rod-shaped structures (Fig. 2) consistent with our previously reported scheme in which pDNA

was regularly folded through the interaction with PEG-polycation block copolymers[34]. The pDNA in the DPc-TPMs then exhibited unique morphological changes depending on the DPc/Asp(DET) ratio. As schematically illustrated in Supplementary Fig. 14, these morphological changes may be explained by considering electrostatic repulsion and ion osmotic pressure in the intermediate compartment. DPc incorporation neutralizes the charge in PAsp(DET), eventually reducing electrostatic repulsion and releasing small counterions to decrease the ion osmotic pressure in the intermediate compartment, thereby leading the polyplex rod to contract to compensate for the interfacial free energy. Further increase in the DPc fraction in the compartment beyond the charge stoichiometry, in turn, generates electrostatic repulsion and increases the ion osmotic pressure, thus extending the polyplex rod. This scheme is in good agreement with the zeta potential profile presented in Supplementary Fig. 5.

Incorporation of DPc into the intermediate layer led to stable pDNA packaging (Fig. 3). In the random-TPM, DPc and pDNA form polyion complexes randomly with PAsp(DET) and PLys, thereby hampering pDNA condensation and placing DPc and pDNA close to each other. However, DPc-TPMs were constructed through the sequential assembly of pDNA, PEG-PAsp(DET)-PLys and DPc; in this way, DPc and pDNA were accommodated into segregated compartments, stably packaging the pDNA. This structural difference also affected the level of pDNA oxidative damage (Supplementary Fig. 9). According to a previous study[35], the lifetime of singlet oxygen (considered to be a major product of an activated PS) is <0.1 ms, and the distance that singlet oxygen can travel in the cell is correspondingly estimated to be 10–20 nm. Considering the length of the PAsp(DET) strand, the distance between DPc and pDNA in DPc-TPMs is estimated to be <20 nm. Thus, singlet oxygen produced in the intermediate layer can reach pDNA in the core compartment. Consistent with these theoretical values, we observed some damage to pDNA. However, because singlet oxygen decays exponentially with time, longer distances between DPc and pDNA are expected to considerably alleviate pDNA damage. Indeed, pDNA in DPc-TPMs exhibited substantially less damage than that in random-TPMs. In addition, in the endo-/lysosomes studied, DPc was released from the DPc-TPMs and localized to lysosomal membranes (Fig. 4), decreasing the amount of DPc in the DPc-TPMs. We confirmed that the decreased amount of DPc reduced the level of oxidative damage (Supplementary Fig. 15). DPc-TPMs (DPc/Asp(DET) = 2) exhibited 69% of the original fluorescence intensity of supercoiled pDNA after photoirradiation at 2 J cm^{-2} (Supplementary Fig. 9); by contrast, DPc-TPMs (DPc/Asp(DET) = 1 and 0.5) exhibited 78% and 85% of the original fluorescence intensity of supercoiled pDNA after photoirradiation at 2 J cm^{-2}, respectively (Supplementary Fig. 15). Thus, the oxidative damage to pDNA experienced during the PCI process inside the cell might be lower than that estimated in this model experiment (Supplementary Fig. 9).

In our *in vitro* study, DPc-TPMs exhibited multistep DPc and pDNA delivery. DPc was delivered to the lysosomal membranes in response to the acidic conditions prevailing in the lysosome, thereby inducing a PCI effect (Fig. 4); pDNA was transferred to the nucleus at high transfection efficiency (Fig. 5 and Supplementary Fig. 11). In our *in vivo* study, more importantly, DPc-TPMs demonstrated light-selective transfection in subcutaneous HeLa and HCT 116 tumours after systemic administration, as shown in Fig. 6 and Supplementary Fig. 13. Although many previous studies have reported systemic nanocarriers for gene delivery into tumours, these nanocarriers inevitably accumulate into highly vascularized normal organs, including lung, liver, spleen and kidney, resulting in non-specific gene expression in these organs. In this regard, spatiotemporal control by PCI is a promising approach for selective gene transfer after systemic administration. Indeed, owing to PCI function in the intermediate layer (Figs 4 and 5 and Supplementary Fig. 11), the DPc-TPMs accomplished light-selective gene expression in the tumour even though some accumulation was observed in normal organs (Supplementary Fig. 12). These results strongly demonstrate the benefit of combining PCI with systemic site-specific gene transduction.

The three-layered micelle concept can be extended to create a universal platform for multistep delivery of therapeutic agents in a spatiotemporally controlled manner. Nanocarrier platforms integrated with such multiple functions offer a promising strategy for overcoming biological barriers (for example, limited extravasation, poor tissue penetration and drug resistance) to treat intractable diseases.

Methods

Synthesis of PEG-PAsp(DET)-PLys triblock copolymer. PEG-PAsp(DET)-PLys triblock copolymer was synthesized as described previously[18] with a minor modification. In brief, as the precursor of PEG-PAsp(DET)-PLys triblock copolymer, PEG-*b*-poly(β-benzyl-L-aspartate)-*b*-poly[ε-(benzyloxycarbonyl)-L-lysine] (PEG-PBLA-PLys(Z)) was synthesized by the sequential ring-opening polymerization of BLA *N*-carboxyanhydride and Lys(Z) *N*-caryboxyanhydride, initiated by α-methoxy-ω-amino-PEG as described previously[18]. The molecular weight distribution (Mw/Mn) of PEG-PBLA-PLys(Z) was determined as 1.05 by gel permeation chromatography, using TOSOH HLC-8220 equipped with TSKgel columns (Super AW4000 and Super AW3000 × 2) and an internal refractive index detector (Tosoh Corporation, Tokyo, Japan). *N*-methyl-2-pyrrolidone containing 50 mM lithium bromide was used as an eluent (flow rate: 0.3 ml min^{-1}; temperature: 40 °C). The amino group of the N-terminal of PEG-PBLA-PLys(Z) was then acetylated using acetic anhydride in dichloromethane. Next, PEG-PBLA-PLys(Z) was lyophilized with benzene and dissolved in *N*-methyl-2-pyrrolidone, after which aminolysis was conducted using diethylenetriamine (50 eq. to the benzyl groups in PBLA) at 0 °C for 1 h. After aminolysis, the solution was neutralized with hydrochloric acid (HCl), dialysed in 0.01 M HCl and lyophilized, followed by microfiltration in water through a 0.02-μm pore-size filter; the residue was then lyophilized. The resulting polymer was dissolved in trifluoroacetic acid, and hydrogen bromide (30% in acetic acid) was added to deprotect the Z groups in the PLys(Z) segment. After 1 h of stirring, the solution was added dropwise into diethyl ether. The resulting precipitate was filtered, dissolved in water, dialysed against 0.01 M HCl and lyophilized to obtain the hydrochloride salt form of PEG-PAsp(DET)-PLys. The DPs of PAsp(DET) and PLys were confirmed using ^{1}H NMR using a JEOL EX300 spectrometer (JEOL Ltd, Tokyo, Japan).

Synthesis of DPc. DPc was synthesized according to a previously reported method[36]. First, dendritic phthalonitrile was obtained by an alkali-mediated coupling reaction of 4-nitrophthalonitrile and a second generation of dendritic phenol. To obtain DPc, the dendritic phthalonitrile was treated with $Zn(OAc)_2$ and 1,8-diazabicyclo[5,4,0]undec-7-ene in *n*-pentanol, followed by treatment with NaOH in a *mixed tetrahydrofuran/*H_2O *solution.*

Preparation of DPc-TPMs. PEG-PAsp(DET)-PLys and pDNA were separately dissolved in 10 mM HEPES (2-[4-(2-hydroxyethyl)-1-piperazinyl]ethanesulphonic acid) buffer (pH 7.3). The polymer solution was then added to a solution of pDNA at a fixed concentration (50 μg ml^{-1}) to form polyplex micelles at a Lys/pDNA ratio of 1. The final concentration of pDNA was fixed at 33.3 μg ml^{-1} for all experiments, except for the ^{1}H NMR, ultracentrifuge, TEM, FRET and *in vivo* experiments. The pDNA/PEG-PAsp(DET)-PLys polyplex micelles were maintained at 4 °C for at least 10 min, after which the DPc solution (in 10 mM HEPES buffer (pH 7.3)) was added at varying DPc/Asp(DET) ratios; the final pDNA concentration was fixed at 30.3 μg ml^{-1}. The protonation degrees of Lys and Asp(DET) units were estimated at pH 7.3 as 1.0 and 0.5, respectively, based on the potentiometric titration results reported in our previous study[19].

^{1}H NMR measurement. Deuterated 10 mM phosphate buffer containing 150 mM NaCl (pH 7.4) was used to prepare the pDNA/PEG-PAsp(DET)-PLys polyplex micelles. pDNA/PEG-PAsp(DET)-PLys polyplex micelles were prepared at a fixed pDNA concentration (166.7 μg ml^{-1}). The measurements of PEG-PAsp(DET)-PLys copolymer (5 mg ml^{-1}) and the polyplex micelles were accumulated 64 and 4,096 times, respectively, at 25 °C using a JEOL EX300 spectrometer (JEOL Ltd).

Gel retardation assay. pDNA and DPc-TPMs were electrophoresed through a 0.9 wt% agarose gel in TAE buffer (3.3 mM Tris-acetic acid (pH 7.4) + 1.7 mM sodium

acetate + 1 mM EDTA/2Na). pDNAs were then stained using 0.5 mg l^{-1} ethidium bromide in distilled water.

Ultracentrifugation. pDNA/PEG-PAsp(DET)-PLys polyplex micelles were prepared at the pDNA concentration of 200 μg ml^{-1}. DPc was then added to the polyplex micelle solution. The final concentration of pDNA was fixed at 182 μg ml^{-1}. The DPc-TPM solution was centrifuged at 62,800 *g* for 2 h (4 °C) to sediment the polyplex micelles using an ultracentrifuge (Optima TLX, Beckman Coulter, Inc., Fullerton, CA, USA). The supernatant was carefully transferred, and the absorption of the supernatant at 670 nm was measured to quantify the amount of DPc not incorporated into the polyplex micelle.

Size and zeta potential of the prepared DPc-TPMs. The size of DPc-TPMs was evaluated by dynamic light scattering at 25 °C using a Zetasizer Nano Series (Malvern Instruments Ltd, Worcestershire, UK) instrument equipped with a laser operating at 532 nm and using a detection angle of 173°. The zeta potential was measured by laser Doppler electrophoresis using a Zetasizer Nano Series instrument equipped with a He–Ne laser (633 nm).

Transmission electron microscopy. DPc-TPMs were prepared at the pDNA concentration of 15.2 μg ml^{-1}. DPc-TPMs at various DPc/Asp(DET) ratios were stained with uranyl acetate and observed using an H-7000 electron microscope (Hitachi Ltd., Tokyo, Japan). The lengths of 100 polyplex micelles were measured using ImageJ software (National Institutes of Health, Bethesda, MD, USA).

FRET experiments. pDNA was labelled with fluorescein and Cy3 using Label IT Tracker Subcellular Nucleic Acid Localization Kits as described previously[22]. Fluorescein and Cy3 were used as the donor–acceptor pair. To form pDNA/PEG-PAsp(DET)-PLys/DPc (DPc-TPM), a solution of PEG-PAsp(DET)-PLys was added to the fluorescein-Cy3-labelled pDNA solution at a fixed concentration (150 μg ml^{-1}) at the Lys/pDNA ratio of 1, after which a DPc solution was added at various DPc/Asp(DET) ratios. The pDNA concentration was fixed at 90.9 μg ml^{-1} in each sample. pDNA/PEG-PLys/DPc diblock-TPMs were prepared in the same manner at a Lys/pDNA ratio of 1.5. To form (pDNA + DPc)/PEG-PAsp(DET)-PLys (random-TPM), pDNA and DPc were mixed at a fixed pDNA concentration (130 μg ml^{-1}), after which a solution of PEG-PAsp(DET)-PLys was added at varying DPc/Asp(DET) ratios. The fluorescence intensity of each sample was measured using a ND-3300 spectrofluorometer (NanoDrop Technologies, Wilmington, DE, USA) with excitation at 470 ± 10 nm. The ratio of fluorescence intensity at 526 nm to that at 569 nm (fluorescein/Cy3) was calculated as a FRET indicator.

Photostability of incorporated pDNA. Forty microlitres of the DPc-TPM solution and 40 μl of the random-TPM solution were photoirradiated using a 300-W halogen lamp (fluence rate, 3.0 mW cm^{-2}) equipped with a band filter (400–700 nm), after which 40 μl of sodium dextran sulphate solution (100 mg ml^{-1}) in 10 mM HEPES buffer (pH 7.3) was added to dissociate the polyplex micelles. The samples were then electrophoresed through a 0.9 wt% agarose gel (running buffer: 3.3 mM Tris-acetic acid (pH 7.4) + 1.7 mM sodium acetate + 1 mM EDTA/2Na). After electrophoresis, pDNAs in the gel were stained using SYBR Green I. The SYBR Green I fluorescence of pDNA was quantified using a Molecular Imager FX Pro (Bio-Rad Laboratories Inc., Hercules, CA, USA) instrument.

Super-resolution imaging of subcellular distributions. The human cervical carcinoma cell line HeLa was obtained from the cell bank of the RIKEN Bioresource Center, Ibaraki, Japan. The cells were grown in DMEM supplemented with 50 μg ml^{-1} penicillin/streptomycin and 10% (v/v) FBS in a 5% CO_2/air incubator at 37 °C. pDNA was labelled with Cy3 using the Label IT Tracker Subcellular Nucleic Acid Localization Kit according to the manufacturer's protocol. In total, 20,000 HeLa cells were seeded on a 35-mm glass-based dish and incubated overnight. After replacing the medium with 1 ml of fresh medium, CellLight Lysosomes–GFP was applied. After 3 days of incubation with CellLight Lysosomes–GFP and medium replacement, a DPc-TPM solution (DPc/Asp(DET) = 1) containing 3 μg of Cy3-labelled pDNA was applied to the cells. After 6 h of incubation, the medium was removed; the cells were then fixed with 4% paraformaldehyde in PBS (phosphate-buffered saline) and observed under an ELYRA PS.1-structured illumination microscope, (Carl Zeiss Inc., Oberkochen, Germany). GFP, Cy3 and DPc were excited using laser light at 488 nm, 561 nm and 642 nm, respectively.

Confocal imaging of PCI. In total, 20,000 HeLa cells were seeded on a 35-mm glass-based dish and incubated overnight. After replacing the medium, CellLight Lysosomes–GFP was applied. After 3 days of incubation with CellLight Lysosomes–GFP and medium replacement, a DPc-TPM solution (DPc/Asp(DET) = 1) containing 3 μg of Cy3-labelled pDNA was applied to the cells. After 6 h of incubation, the medium was replaced, and the cells were photoirradiated at a fluence of 2 J cm^{-2} using a 300-W halogen lamp (fluence rate, 3.0 mW cm^{-2}) equipped with a band filter (400–700 nm). The photoirradiated cells were then incubated for an additional 3.5 h, after which the subcellular distribution of DPc-TPMs was observed using a CLSM, LSM 780 (Carl Zeiss Inc.) instrument, equipped with an incubator (Tokai Hit Co., Ltd, Shizuoka, Japan), thereby maintaining the temperature at 36.5 °C under a humidified atmosphere containing 5% CO_2/air. GFP and Cy3 were excited with laser light at 488 nm and 561 nm, respectively. The emission wavelengths of GFP and Cy3 were set to 489–551 nm and 568–629 nm, respectively. The acquisition interval used in the time-series imaging was set to 15 min. The data obtained in the time-series imaging were analysed using Imaris software (Bitplane, Zurich, Switzerland) to estimate the PCC between GFP and Cy3.

***In vitro* transfection and cytotoxicity assays.** In total, 10,000 HeLa cells per well were plated on 24-well plates 24 h before transfection. The cells were then incubated with DPc-TPMs or diblock-TPMs containing 1 μg of pDNA. After 6 h of incubation at 37 °C, the cells were washed with PBS, after which the medium was replaced. The cells were then irradiated using a 300-W halogen lamp (fluence rate, 3.0 mW cm^{-2}) equipped with a band filter (400–700 nm). After an additional 40 h of incubation following photoirradiation, the cells were washed with PBS and lysed with 200 μl of Cell-LyEX 1 per well. Luciferase gene expression was evaluated using LB940 (Berthold Technologies, Bad Wildbad, Germany) or Glomax (Promega). The amount of protein in each well was determined using a Micro BCA Protein Assay Reagent Kit. Cell viability was evaluated using the 3-(4,5-dimethylthiazol-2-yl)-2,5-diphenyltetrazolium bromide (MTT) assay.

***In vivo* transfection.** Female 5-week-old C.B-17 severe combined immunodeficiency (SCID) mice and female 5-week-old BALB/c nude mice were obtained from Charles River Laboratories Japan Inc. (Kanagawa, Japan). All animal experiments were performed in accordance with the Guidelines for the Care and Use of Laboratory Animals as stated by the University of Tokyo. HeLa cells were inoculated into a C.B-17 SCID mouse. The resulting tumours were then subcutaneously transplanted into BALB/c nude mice. When the tumour size reached ~100 mm^3, 220 μl of a DPc-TPM solution containing pDNA encoding Venus at a DPc/Asp(DET) ratio of 1 (182 μg ml^{-1} of pDNA) was intravenously injected. Twenty-four hours after injection, the mice were anesthetized with isoflurane (Abbott Japan Co., Ltd, Tokyo, Japan), and the tumour sites were irradiated with a diode laser at 680 nm (maximum output: 2 W, numerical aperture: 0.22, B&W TEK, Newark, DE, USA) at a dose of 12 J cm^{-2}. Three days after photoirradiation, Hoechst 33342 (5 mg kg^{-1} in PBS) was intravenously injected to stain the nuclei. The tumours were then excised and observed using a Nikon A1R CLSM (Nikon Corp., Tokyo, Japan). Hoechst 33342 and Venus were excited with laser light at 405 nm and 488 nm, respectively. The emission wavelengths of Hoechst 33342 and Venus were set to 425–475 nm and 500–550 nm, respectively. Image processing was performed using Nikon NIS Elements software (Nikon Corp.). Venus fluorescence was quantified by subtraction of the background intensity from the mean fluorescence intensity of each image. The background intensity was obtained from the image of a tumour excised from a non-treated tumour-bearing mouse. The average Venus fluorescence intensity in each mouse was calculated from eight images, and the mean fluorescent intensities and standard errors were calculated from five mice for tumours without photoirradiation, and from six mice for tumours with photoirradiation.

References

1. Duncan, R. The dawning era of polymer therapeutics. *Nat. Rev. Drug Discov.* **2,** 347–360 (2003).
2. Peer, D. *et al.* Nanocarriers as an emerging platform for cancer therapy. *Nat. Nanotech.* **2,** 751–760 (2007).
3. Kim, B. Y. S., Rutka, J. T. & Chan, W. C. W. Current concepts: Nanomedicine. *New Engl. J. Med.* **363,** 2434–2443 (2010).
4. Cabral, H., Nishiyama, N. & Kataoka, K. Supramolecular nanodevices: from design validation to theranostic nanomedicine. *Acc. Chem. Res.* **44,** 999–1008 (2011).
5. Bourzac, K. Nanotechnology: carrying drugs. *Nature* **491,** S58–S60 (2012).
6. Miyata, K., Nishiyama, N. & Kataoka, K. Rational design of smart supramolecular assemblies for gene delivery: chemical challenges in the creation of artificial viruses. *Chem. Soc. Rev.* **41,** 2562–2574 (2012).
7. Rai, P. *et al.* Development and applications of photo-triggered theranostic agents. *Adv. Drug Deliv. Rev.* **62,** 1094–1124 (2010).
8. Tachibana, K., Feril, L. B. & Ikeda-Dantsuji, Y. Sonodynamic therapy. *Ultrasonics* **48,** 253–259 (2008).
9. Plank, C., Zelphati, O. & Mykhaylyk, O. Magnetically enhanced nucleic acid delivery. Ten years of magnetofection-progress and prospects. *Adv. Drug Deliv. Rev.* **63,** 1300–1331 (2011).
10. Palumbo, G. Photodynamic therapy and cancer: a brief sightseeing tour. *Expert Opin. Drug Deliv.* **4,** 131–148 (2007).

11. O'Connor, A. E., Gallagher, W. M. & Byrne, A. T. Porphyrin and nonporphyrin photosensitizers in oncology: preclinical and clinical advances in photodynamic therapy. *Photochem. Photobiol.* **85,** 1053–1074 (2009).
12. Agostinis, P. *et al.* Photodynamic therapy of cancer: An update. *CA Cancer J. Clin.* **61,** 250–281 (2011).
13. Høgset, A. *et al.* Photochemical internalisation in drug and gene delivery. *Adv. Drug Deliv. Rev.* **56,** 95–115 (2004).
14. Berg, K. *et al.* Photochemical internalization: a new tool for drug delivery. *Curr. Pharm. Biotechnol.* **8,** 362–372 (2007).
15. Norum, O. J., Selbo, P. K., Weyergang, A., Giercksky, K. E. & Berg, K. Photochemical internalization (PCI) in cancer therapy: from bench towards bedside medicine. *J. Photochem. Photobiol. B* **96,** 83–92 (2009).
16. Berg, K. *et al.* Disulfonated tetraphenyl chlorin ($TPCS_{2a}$), a novel photosensitizer developed for clinical utilization of photochemical internalization. *Photochem. Photobiol. Sci.* **10,** 1637–1651 (2011).
17. Miyata, K., Fukushima, S., Nishiyama, N., Yamasaki, Y. & Kataoka, K. PEG-based block catiomers possessing DNA anchoring and endosomal escaping functions to form polyplex micelles with improved stability and high transfection efficacy. *J. Control. Release* **122,** 252–260 (2007).
18. Miyata, K. *et al.* Polyplex micelles from triblock copolymers composed of tandemly aligned segments with biocompatible, endosomal escaping, and DNA-condensing functions for systemic gene delivery to pancreatic tumor tissue. *Pharm. Res.* **25,** 2924–2936 (2008).
19. Miyata, K. *et al.* Polyplexes from poly(aspartamide) bearing 1,2-diaminoethane side chains induce pH-selective, endosomal membrane destabilization with amplified transfection and negligible cytotoxicity. *J. Am. Chem. Soc.* **130,** 16287–16294 (2008).
20. Herlambang, S. *et al.* Disulfide crosslinked polyion complex micelles encapsulating dendrimer phthalocyanine directed to improved efficiency of photodynamic therapy. *J. Control. Release* **155,** 449–457 (2011).
21. Itaka, K., Harada, A., Nakamura, K., Kawaguchi, H. & Kataoka, K. Evaluation by fluorescence resonance energy transfer of the stability of nonviral gene delivery vectors under physiological conditions. *Biomacromolecules* **3,** 841–845 (2002).
22. Matsumoto, Y., Itaka, K., Yamasoba, T. & Kataoka, K. Intranuclear fluorescence resonance energy transfer analysis of plasmid DNA decondensation from nonviral gene carriers. *J. Gene Med.* **11,** 615–623 (2009).
23. Nishiyama, N. *et al.* Light-induced gene transfer from packaged DNA enveloped in a dendrimeric photosensitizer. *Nat. Mater.* **4,** 934–941 (2005).
24. MacDonald, I. J. & Dougherty, T. J. Basic principles of photodynamic therapy. *J. Porphyrins Phthalocyanines* **5,** 105–129 (2001).
25. Cabral, H. *et al.* A photo-activated targeting chemotherapy using glutathione sensitive camptothecin-loaded polymeric micelles. *Pharm. Res.* **26,** 82–92 (2008).
26. de Bruin, K. G. *et al.* Dynamics of photoinduced endosomal release of polyplexes. *J. Control. Release* **130,** 175–182 (2008).
27. Oliveira, S., Høgset, A., Storm, G. & Schiffelers, M. Delivery of siRNA to the target cell cytoplasm: photochemical internalization facilitates endosomal escape and improves silencing efficiency, *in vitro* and *in vivo*. *Curr. Pharm. Des.* **14,** 3686–3697 (2008).
28. Akagi, D. *et al.* Biocompatible micellar nanovectors achieve efficient gene transfer to vascular lesions without cytotoxicity and thrombus formation. *Gene Ther.* **14,** 1029–1038 (2007).
29. Itaka, K. *et al.* Bone regeneration by regulated *in vivo* gene transfer using biocompatible polyplex nanomicelles. *Mol. Ther.* **15,** 1655–1662 (2007).
30. Harada-Shiba, M. *et al.* Intratracheal gene transfer of adrenomedullin using polyplex nanomicelles attenuates monocrotaline-induced pulmonary hypertension in rats. *Mol. Ther.* **17,** 1180–1186 (2009).
31. Oba, M. *et al.* Antiangiogenic gene therapy of solid tumor by systemic injection of polyplex micelles loading plasmid DNA encoding soluble Flt-1. *Mol. Pharm.* **7,** 501–509 (2010).
32. Vachutinsky, Y. *et al.* Antiangiogenic gene therapy of experimental pancreatic tumor by sFlt-1 plasmid DNA carried by RGD-modified crosslinked polyplex micelles. *J. Control. Release* **149,** 51–57 (2011).
33. Chen, Q. *et al.* Homo-catiomer integration into PEGylated polyplex micelle from block-catiomer for systemic anti-angiogenic gene therapy for fibrotic pancreatic tumors. *Biomaterials* **33,** 4722–4730 (2012).
34. Osada, K. *et al.* Enhanced gene expression promoted by the quantized folding of pDNA within polyplex micelles. *Biomaterials* **33,** 325–332 (2012).
35. Moan, J. & Berg, K. The photodegradation of porphyrins in cells can be used to estimate the lifetime of singlet oxygen. *Photochem. Photobiol.* **53,** 549–553 (1991).
36. Ng, A. C. H., Li, X. Y. & Ng, D. K. P. Synthesis and photophysical properties of nonaggregated phthalocyanines bearing dendritic substituents. *Macromolecules* **32,** 5292–5298 (1999).

Acknowledgements

This work was partially supported by Funding Program for World-Leading Innovative R&D on Science and Technology (FIRST Program) from Japan Society for the Promotion of Science (JSPS), Center of Innovation (COI) Program, the Core Research Program for Evolutional Science and Technology (CREST), and Precursory Research for Embryonic Science and Technology (PRESTO) from Japan Science and Technology Agency (JST). This work was also supported by Grant-in-Aid for JSPS Fellows from JSPS and Takeda Science Foundation.

Author contributions

T.N. designed and performed all the experiments and wrote the manuscript; S.F. assisted with the polymer synthesis and characterization of the micelles; M.K. and K.Ma. assisted with characterization of the micelles; A. conducted preliminary experiments; Y.M. helped in the FRET study and super-resolution microscopy; M.O. and K.Mi. advised on the *in vitro* and *in vivo* study; K.O. advised on characterization of the micelles; N.N. and K.K. edited the manuscript and supervised the whole project.

Additional information

Supplementary Information accompanies this paper at http://www.nature.com/naturecommunications

Competing financial interests: The authors declare no competing financial interests.

Reprints and permission information is available online at http://npg.nature.com/reprintsandpermissions/

How to cite this article: Nomoto, T. *et al.* Three-layered polyplex micelle as a multifunctional nanocarrier platform for light-induced systemic gene transfer. *Nat. Commun.* 5:3545 doi: 10.1038/ncomms4545 (2014).

Biochemical and Biophysical Research Communications 458 (2015) 470–475

Contents lists available at ScienceDirect

Biochemical and Biophysical Research Communications

journal homepage: www.elsevier.com/locate/ybbrc

Physical interaction between MPP8 and PRC1 complex and its implication for regulation of spermatogenesis

Kazuhiro Murata [a], Shinya Sato [b], Mayumi Haruta [a], Takahiro Goshima [a], Yoshie Chiba [a], Satoru Takahashi [b], Jafar Sharif [c], Haruhiko Koseki [c], Makoto Nakanishi [a, *], Midori Shimada [a, *]

[a] Department of Cell Biology, Graduate School of Medical Sciences, Nagoya City University, 1 Kawasumi, Mizuho-cho, Mizuho-ku, Nagoya, 467-8601, Japan
[b] Experimental Pathology and Tumor Biology, Graduate School of Medical Sciences, Nagoya City University, 1 Kawasumi, Mizuho-cho, Mizuho-ku, Nagoya, 467-8601, Japan
[c] Development Genetics Group, RIKEN Center for Integrative Medical Sciences (IMS), 1-7-22 Suehiuro-cho, Tsurumi, Yokohama, Kanagawa, 230-0045, Japan

ARTICLE INFO

Article history:
Received 17 January 2015
Available online 7 February 2015

Keywords:
Epigenetics
Transcription
Spermatocyte
Differentiation

ABSTRACT

Epigenetic modifications such as DNA methylation and histone H3 lysine 27 methylation (H3K27me) are repressive marks that silence gene expression. The M phase phosphoprotein (MPP8) associates with proteins involved in both DNA methylation and histone modifications, and therefore, is a potential candidate to mediate crosstalk between repressive epigenetic pathways. Here, by performing immunohistochemical analyses we demonstrate that MPP8 is expressed in the rodent testis, especially in spermatocytes, suggesting a role in spermatogenesis. Interestingly, we found that MPP8 physically interacts with PRC1 (Polycomb Repressive Complex 1) components which are known to possess essential function in testis development by modulating monoubiquitination of Histone H2A (uH2A) and trimethylation of Histone H3 Lysine 27 (H3K27me3) residues. Knockdown analysis of MPP8 in HeLa cells resulted in derepression of a set of genes that are normally expressed in spermatogonia, spermatids and mature sperm, thereby indicating a role for this molecule in silencing testis-related genes in somatic cells. In addition, depletion of MPP8 in murine ES cells specifically induced expression of genes involved in mesoderm differentiation, such as Cdx2 and Brachyury even in the presence of LIF, which implicated that MPP8 might be required to repress differentiation associated genes during early development. Taken together, our results indicate that MPP8 could have a role for silencing genes that are associated with differentiation of the testis and the mesoderm by interacting with epigenetic repressors modules such as the PRC1 complex.

1. Introduction

The M phase phosphoprotein 8 (MPP8) was identified as a protein that is highly phosphorylated during M phase [1]. MPP8 possesses a chromodomain in the amino terminal region which has an affinity for trimethylated histone H3 lysine 9 (H3K9me3) residues [5,6]. This chromodomain also binds to dimethylated Dnmt3a (K44me2), a mammalian *de novo* DNA methyltransferase, and auto-methylated GLP or G9a, both of which are linked with H3K9 dimethylation [2]. Given that the MPP8 chromodomain forms a dimmer in solution [3], it is possible that this protein could play a role as a scaffold to form a multimeric silencing complex comprising of Dnmt3a-MPP8-GLP/G9a to regulate chromatin templates [2]. During cell cycle progression, MPP8 predominantly localizes to chromatin, but dissociates during interphase and early mitosis, respectively, although its expression appeared to be constant [7]. Chromatin dissociation of MPP8 during M phase is regulated by at least in part by cyclin B1-Cdk1-dependent phosphorylation [7]. Importantly, tissue-specific expression of MPP8 in mice revealed a predominant expression pattern in testis and far lower ubiquitous expression in most of the tissues, suggesting that this protein could have a role during spermatogenesis.

* Corresponding authors. Fax: +81 52 842 3955.
E-mail addresses: mkt-naka@med.nagoya-cu.ac.jp (M. Nakanishi), midorism@med.nagoya-cu.ac.jp (M. Shimada).

http://dx.doi.org/10.1016/j.bbrc.2015.01.122
0006-291X/